Hydrologic and geomorphic controls on hyporheic exchange during base flow recession in a headwater mountain stream

Adam S. Ward,[1,2] Michael Fitzgerald,[3] Michael N. Gooseff,[1] Thomas J. Voltz,[1] Andrew M. Binley,[4] and Kamini Singha[3]

Received 29 September 2011; revised 16 February 2012; accepted 4 March 2012; published 13 April 2012.

[1] Hyporheic hydrodynamics are a control on stream ecosystems, yet we lack a thorough understanding of catchment controls on these flow paths, including valley constraint and hydraulic gradients in the valley bottom. We performed four whole-stream solute tracer injections under steady state flow conditions at the H. J. Andrews Experimental Forest (Oregon, United States) and collected electrical resistivity (ER) imaging to directly quantify the 2-D spatial extent of hyporheic exchange through seasonal base flow recession. ER images provide spatially distributed information that is unavailable for stream solute transport modeling studies from monitoring wells alone. The lateral and vertical extent of the hyporheic zone was quantified using both ER images and spatial moment analysis. Results oppose the common conceptual model of hyporheic "compression" by increased lateral hydraulic gradients toward the stream. We found that the extent of the hyporheic zone increased with decreasing vertical gradients away from the stream, in contrast to expectations from conceptual models. Increasing hyporheic extent was observed with both increasing and decreasing down-valley (i.e., parallel to the valley gradient) and cross-valley (i.e., from the hillslope to the stream, perpendicular to the valley gradient) hydraulic gradients. We conclude that neither cross-valley nor down-valley hydraulic gradients are sufficient predictors of hyporheic exchange flux nor flow path network extent. Increased knowledge of the controls on hyporheic exchange, the temporal dynamics of exchange flow paths, and their the spatial distribution is the first step toward predicting hyporheic exchange at the scale of individual flow paths. Future studies need to more carefully consider interactions between spatiotemporally dynamic hydraulic gradients and subsurface architecture as controls on hyporheic exchange.

Citation: Ward, A. S., M. Fitzgerald, M. N. Gooseff, T. J. Voltz, A. M. Binley, and K. Singha (2012), Hydrologic and geomorphic controls on hyporheic exchange during base flow recession in a headwater mountain stream, *Water Resour. Res.*, *48*, W04513, doi:10.1029/2011WR011461.

1. Introduction

[2] Linking the transport of solutes along hyporheic flow paths with dynamic hydrologic processes occurring at the catchment scale remains a challenge. However, the physical processes controlling the individual aspects of catchment hydrology, and riparian hydrology and hydraulics have been relatively well studied as discrete processes. In particular, hyporheic exchange (i.e., the movement of water between the stream and near-stream aquifer over relatively short spatial and temporal scales) has been well characterized at the channel unit to subreach scales (tens to hundreds of meters). While a comprehensive understanding of how catchments and streams control hyporheic exchange is lacking, it is recognized that hyporheic hydrodynamics are the setting upon which biogeochemical cycling in the subsurface occurs [e.g., *Battin*, 1999, 2000; *Boano et al.*, 2010; *Zarnetske et al.*, 2011]. To advance our understanding of biogeochemical cycling, we must improve our ability to resolve hydrodynamic subsurface processes [e.g., *Bencala et al.*, 2011; *Hanrahan*, 2008; *Wondzell et al.*, 2009].

[3] Streambed morphology, hydrogeologic setting, and hydrodynamics are recognized as the three primary controls on hyporheic exchange. First, streambed morphology controls hyporheic exchange. At the scale of channel bedforms (e.g., dunes) pressure variations generate a pumping exchange [e.g., *Cardenas and Wilson*, 2007a; *Elliott and Brooks*, 1997a, 1997b; *Savant et al.*, 1987]. Hydrostatic pressure differentials around larger geomorphologic features (i.e., pools, riffles, and steps) generate suites of hyporheic flow paths extending both vertically and laterally from the stream [e.g., *Gooseff et al.*, 2006; *Harvey and Bencala*, 1993; *Kasahara and Wondzell*, 2003]. In addition to the exchanges described above, hyporheic flow paths may also be defined as occurring in the lateral dimension

[1]Department of Civil and Environmental Engineering, Pennsylvania State University, University Park, Pennsylvania, USA.
[2]Now at Department of Geoscience, University of Iowa, Iowa City, Iowa, USA.
[3]Department of Geosciences, Pennsylvania State University, University Park, Pennsylvania, USA.
[4]Lancaster Environment Centre, Lancaster University, Lancaster, UK.

0043-1397/12/2011WR011461

from the stream (e.g., flow through a meander bend or point bar) [e.g., *Peterson and Sickbert*, 2006; *Revelli et al.*, 2008; *Zarnetske et al.*, 2011].

[4] The geologic setting of a stream is the second primary control on hyporheic exchange, setting the template upon which exchange may occur [*Wondzell and Gooseff*, 2012]. *Valett et al.* [1996] demonstrated the relationship between parent lithology and hyporheic exchange with solute tracer studies in three different geologic settings. Indeed, the distribution of hydrogeologic properties of the subsurface has been demonstrated as a control on hyporheic exchange at scales including the bedding of grains [*Sawyer and Cardenas*, 2009], heterogeneous distributions of hydraulic conductivity within layers [e.g., *Packman and Salehin*, 2003; *Salehin et al.*, 2004], and macroscale heterogeneities in the subsurface [e.g., *Ryan and Boufadel*, 2006; *Vaux*, 1968; *Ward et al.*, 2011]. In particular, highly constrained valleys (i.e., those where bedrock or other subsurface features restrict the extent of an alluvial deposit, and therefore a hyporheic zone) have been associated with reduced hyporheic residence times, smaller hyporheic zones, and restricted hyporheic exchange [e.g., *D'Angelo et al.*, 1993; *Stanford and Ward*, 1993; *Wright et al.*, 2005]. Indeed, recent numerical studies demonstrate the effect of subsurface architecture on hyporheic flow path network extent and residence time [*Ward et al.*, 2012].

[5] The third control on hyporheic exchange is hydraulic gradients between the stream and adjacent landscape. Riparian hydrology exists as a buffer between boundaries set by large-scale, relatively slow-moving processes at the hillslope, catchment, or regional setting and more dynamic processes occurring in the stream channel. *Burt* [2005, pp. 2087–2088] notes that "the riparian zone is perhaps the most important element of the hydrological landscape given that it can decouple the linkage between the major landscape elements, hillslope and channel." While *Larkin and Sharp* [1992] demonstrated that stream-groundwater interactions throughout catchments can be considered a function of channel slope, sinuosity, incision, and aspect ratio, few studies have considered hyporheic hydrology, in which some portion of the riparian zone is composed of stream water traveling along hyporheic flow paths. Indeed, the view of riparian hydrology as a function of its boundaries is prevalent in the literature [e.g., *Vidon and Hill*, 2004]. As a boundary condition, increasing streamflow may increase hyporheic exchange rates [e.g., *Elliott and Brooks*, 1997a, 1997b; *Fabian et al.*, 2010; *Hart et al.*, 1999; *Packman and Salehin*, 2003]. Stream solute transport simulations subsequent to tracer studies conducted at the reach scale generally note that the ratio of storage zone area to stream area (commonly A_S/A) decreases with increasing flow [*Butturini and Sabater*, 1999; *Fabian et al.*, 2010; *Karwan and Saiers*, 2009; *Morrice et al.*, 1997; *Schmid et al.*, 2010; *Zarnetske et al.*, 2007], though others have found little correlation [*Hart et al.*, 2002; *Schmid et al.*, 2010] or increases with increasing flow [*Fabian et al.*, 2010; *Morrice et al.*, 1997; *Wondzell*, 2006]. Groundwater discharge to streams has widely been theorized to restrict the spatial extent of hyporheic flow paths [e.g., *Hakenkamp et al.*, 1993; *Hynes*, 1983; *Meyer et al.*, 1988; *Palmer*, 1993; *Vervier et al.*, 1992; *White*, 1993]. In contrast, *Wondzell* [2006] completed replicate tracer studies in two steep headwater catchments in the H. J. Andrews Experimental Forest under different base flow conditions, finding that hyporheic extent, evaluated as tracer arrival in a riparian monitoring well network, did not change throughout base flow recession. Spatiotemporal variability in stream and hillslopes hydraulics have been studied as a control on hyporheic exchange, yet we lack a complete perspective of interactions between riparian hydrodynamics and hyporheic exchange.

[6] Solute tracer experiments are commonly employed to characterize hyporheic exchange and extent [*Stream Solute Workshop*, 1990], with field observations typically interpreted using simple solute transport models that simulate time series of stream tracer concentrations [e.g., *Bencala and Walters*, 1983; *Briggs et al.*, 2008; *Choi et al.*, 2000; *Runkel*, 1998]. However, model interpretations provide only spatially lumped characterizations of only a subset of subsurface flow paths (i.e., those within the study's window of detection, generally the shortest residence times) [e.g., *Gooseff et al.*, 2003; *Harvey et al.*, 1996; *Harvey and Wagner*, 2000]. Further, stream solute transport model results are sensitive to exchange with other slow moving water in streams (i.e., surface transient storage zones [e.g., *Briggs et al.*, 2008]). Shallow monitoring wells have been used to sample hyporheic water, but they provide spatially discrete point measurements of tracer in the subsurface, since an individual well is only sensitive to those of flow paths that intercept its location. Hence, there is significant mismatch between well observations and stream solute-transport model simulations [e.g., *Harvey et al.*, 1996; *Wondzell*, 2006]. In response to the need for increased spatial and temporal resolution in monitoring hyporheic exchange, *Ward et al.* [2010] demonstrated that the use of electrical resistivity (ER) imaging coupled with electrically conductive solute tracers could be used to image hyporheic flow paths in two dimensions across stream transects. Here we apply this technique to study valley-bottom hydrology during base flow recession.

[7] The objective of this study is to assess the roles of changing hydrologic conditions during base flow recession and valley constraint as controls on hyporheic exchange. We seek to answer the questions: How does hyporheic extent change as a function of valley constraint?, and How does hyporheic extent change as a function of changing hydrologic forcing during base flow recession? Based on our review of the literature, we expect: hyporheic flow path networks will spatially expand during base flow recession due to gradients decreasing in magnitude from the hillslopes toward the stream; hyporheic extent (defined for this study as both the vertical and lateral dimensions of the flow path network, perpendicular to the stream) will be most consistent through time in locations where valley constraint is largest, because subsurface controls (i.e., hydrogeologic properties, confining units) dominate hydraulic gradient controls; and hyporheic extent will be greatest in locations and during periods where down-valley gradients are largest, because steeper down-valley gradients drive more down-valley subsurface flow and will enable flow path network expansion. To test these hypotheses we conducted four replicate solute tracer studies in a study reach including a laterally constrained upper section and a less-constrained lower section during base flow recession. Tracer concentrations were monitored in-stream, in monitoring

wells, and using electrical resistivity imaging. A suite of associated hydrological data were also collected to characterize vertical, cross-valley, and down-valley hydraulic gradients within the riparian zone. These assessment techniques provide superior spatial resolution in the subsurface and temporal resolution through the base flow recession period, allowing us to link hyporheic exchange with dynamic valley-bottom boundary conditions (i.e., in-stream flow and hydraulic gradients from the hillslopes to the stream).

2. Methods

2.1. Site Description

[8] Field studies were completed at the H. J. Andrews Experimental Forest, located in the western Cascade Mountains of Oregon, United States (48°10′N, 122°15′W). Studies were conducted in WS3, a steep headwater catchment draining 101 ha. Flow at the watershed outlet ranged from 4 to 35 L s^{-1} during the study period. Hillslope gradients greater than 50% constrain a narrow valley bottom. The watershed ranges in elevation from 497 to 1070 m above mean sea level. Soils are generally shallow loams (1–2 m) with high porosities and infiltration rates [*Dyrness*, 1969]. *Wondzell et al.* [2009] report a saturated hydraulic conductivity of 1.7×10^{-5} m s^{-1} as the geometric mean of slug tests in the riparian soils of an adjacent watershed (WS1, a nearby catchment), while *Kasahara and Wondzell* [2003] report an average value of 7×10^{-5} m s^{-1} for WS3 and WS1 combined.

[9] A highly instrumented study reach of ~40 m was established (Figure 1A). The second-order stream has a 14% mean topographic gradient through the study reach.

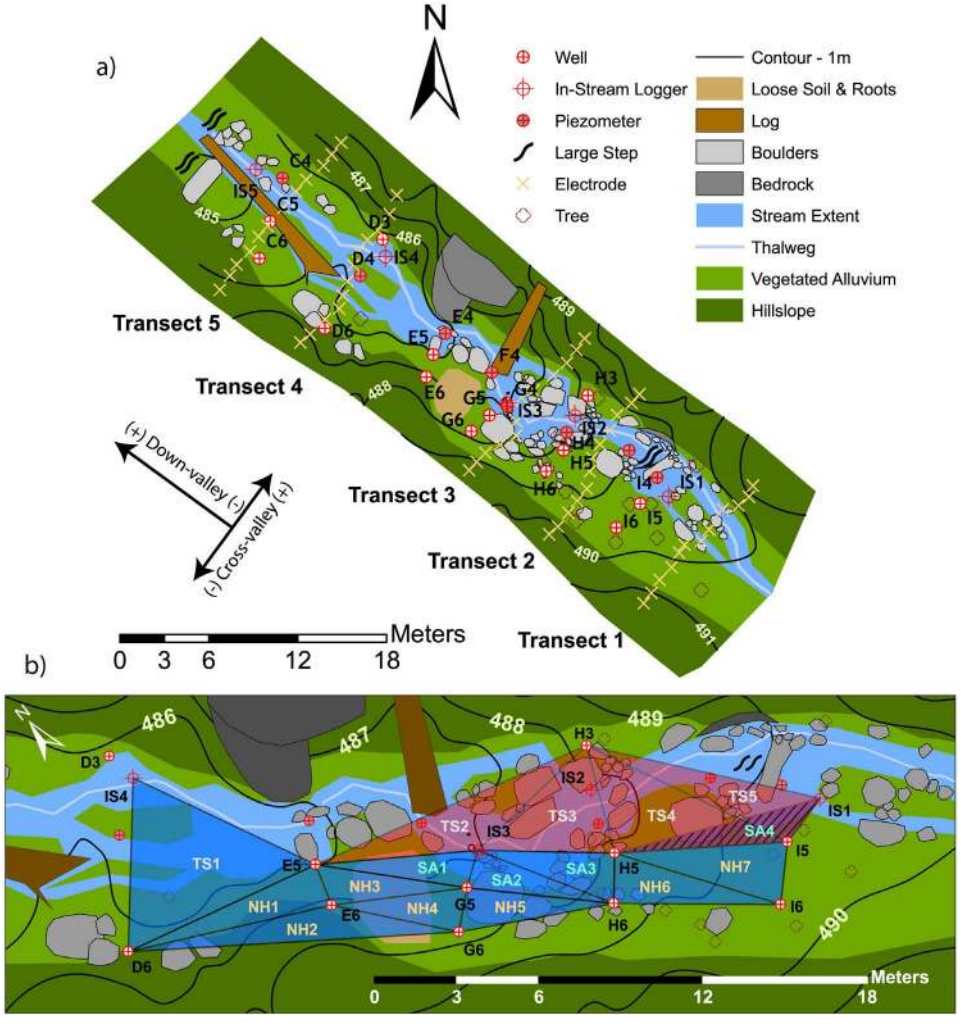

Figure 1. Site location and instrumentation maps for (a) WS3 in the H. J. Andrews Experimental Forest, located in the Cascade Range of central Oregon. Piezometers and well transects are organized by letter (from C downstream to I upstream) and number (increasing from north to south across the valley); in-stream observations are identified by the prefix IS and location number. (b) Triangular elements uspoed for analysis of riparian hydraulic gradients in WS3, representing the maximum number of data that can be independently obtained from the instrumented well network. Each of the finite elements is classified as through-stream (TS), stream-adjacent (SA), or near-hillslope (NH), and assigned a number to uniquely identify each element. Blue elements were monitored for the entire season; red elements were monitored for only part of the season. (Modified from Figures 2–3 and 4–3 by *Voltz* [2011]).

Stream morphology is a sequence of pools, riffles, and steps. An average of 8.4 steps or riffles per 100 m of stream length contributes 54% of the elevation change along the stream [*Kasahara and Wondzell*, 2003].

[10] WS3 is a narrow valley (5 m average, 9 m maximum valley bottom width), described as bedrock-constrained by *Wondzell* [2006]. The upper end of the study reach (ER transects 1–3) is highly constrained, with the stream against the steep bedrock wall on the north side of the valley. The valley slope averages 16% through this upper study reach. In contrast, the lower portion of the study reach (ER transects 4–5) is in a flatter (6% valley slope) and wider (9 m width) valley bottom. A larger alluvial deposit exists across the width of the valley in this segment, held in place by boulders and logs that span the valley width.

2.2. Hydrologic Observations

[11] Flow rate at the outlet of WS3 is gauged using a permanently installed weir maintained by the U. S. Forest Service. WS3 contains a network of 17 shallow monitoring wells and eight piezometers installed in 1997. Wells and piezometers are hand-driven lengths of PVC, with maximum penetration of 1.7 m (<1 m in many locations). Wells were screened over the bottom 50 cm by drilling 0.32 cm diameter holes, with an approximate density of one hole per 4 cm^2. Piezometers were screened with the same size holes and density over the bottom 5 cm only. *Wondzell* [2006] provides additional details about well installation and network layout. The potentiometric surface was recorded using pressure transducers and water level capacitance rods in a subset of the well network (13 wells and eight piezometers) and at five locations in the stream channel.

[12] Water surface elevations observed in the stream and monitoring wells were used to construct potentiometric surface maps at 30-min intervals for the study period by linearly interpolating between measurement locations on a 25-cm grid. The area of analysis was clipped to only include the riparian and hillslope areas bounded by the monitoring well network and on the south side of the stream centerline. For each grid point the cross-valley gradient (i.e., gradient perpendicular to the down-valley axis) and down-valley gradient (i.e., the gradient parallel to the down-valley axis) magnitudes were calculated. The cross-valley gradient is positive for gradients sloping in the northeast direction (i.e., toward the stream), and negative for gradients sloping in the southwest direction (Figure 1A). The interpolated 25-cm grid data were used to calculate the valley bottom average cross-valley and down-valley gradients. Additionally, observation locations were used to construct a triangular grid consisting of 16 triangular elements covering the valley bottom (Figure 1B). Cross-valley and down-valley gradients for each element were calculated at 30-min intervals for the study period. The triangular grid was divided into elements that extended through the stream itself ("through-stream," or TS), in the riparian area adjacent to the stream ("stream-adjacent," SA), and those near the hillslopes ("near-hillslope," or NH).

[13] Water surface observations in the stream and piezometer network were used to calculate vertical hydraulic gradients at two locations. Vertical hydraulic gradient (VHG, m m^{-1}) was calculated as,

$$\mathrm{VHG} = \frac{h_{\mathrm{stream}} - h_{\mathrm{piezometer}}}{e_{\mathrm{streambed}} - e_{\mathrm{tos}}}, \tag{1}$$

where h_{stream} and $h_{\mathrm{piezometer}}$ are the head in the stream and piezometer, $e_{\mathrm{streambed}}$ is the streambed elevation, and e_{tos} is the elevation of the top of the piezometer screen (after *Baxter et al.* [2003]; *Wondzell* [2006]). VHG is positive in upwelling locations and negative in downwelling locations.

2.3. Solute Tracer Studies

[14] Four 48-h constant-rate injections of sodium chloride (NaCl, an assumed conservative tracer) were completed at the same location used by *Wondzell* [2006] (~50 m upstream of the study reach). A concentrated NaCl solution was injected at a constant rate directly into the stream channel; injections were designed to increase in-stream electrical conductivity (EC) by 100 μS cm^{-1} from background levels of ~40 μS cm^{-1}. EC was used as a surrogate for tracer concentration in all measurements [*Baxter et al.*, 2003; *Gooseff and McGlynn*, 2005; *Payn et al.*, 2009; *Wondzell*, 2006]. For all studies, injections began between 13:00 and 14:00.

[15] Electrical conductivity of surface water was recorded in the stream channel using temperature and EC probes manufactured by Campbell Scientific, Inc. (Logan, Utah, United States) at a well-mixed stream reach near the upstream end of the study reach (IS1 in Figure 1A). Electrical conductivity was also monitored in the well network during the study. The well-sampling procedure was to purge at least one well volume using a manual siphon and measure EC using either an EcoSense EC300 (YSI, Inc., Yellow Springs, Ohio, United States) or a model 107 Temperature/Level/Conductivity meter (Solinst, Inc., Georgetown, Ontario, Canada) deployed down the well.

2.4. Electrical Resistivity Imaging

2.4.1. Data Collection

[16] Electrical resistivity data were collected using a 10-channel Syscal Pro Resistivity Meter (IRIS Instruments, Orleans, France). Data were collected on a network of electrodes installed in five transects oriented perpendicular to the valley (T1–3 during injection 1; T1–5 for injections 2–4), spaced ~5 m apart along the study reach. Electrodes were positioned within each transect across the stream using a variable spacing layout where electrodes in the valley bottom and stream portion of the site were positioned with ~1 m spacing laterally in the valley bottom, and a maximum of 2 m in the hillslopes (Figure 1A). This arrangement was selected to yield high-resolution measurements in the valley bottom, where the greatest changes in EC were expected.

[17] Electrodes were manufactured from 1.27-cm diameter PVC pipes ~0.75 m in length. Conductive foil tape was wrapped around the pipe ~10 cm from the bottom. An 18-gauge stranded wire connected the foil tape (i.e., contact surface below ground) to the trunk line of wires (solid strand 18 gauge), which connected to the ER switch box. Contact resistance of the electrodes was checked with the Syscal Pro prior to each injection and periodically during

the ER monitoring period. Contact resistance values ranged from 1 to 16 kΩ with about 90% lower than 5 kΩ for the entire duration of each monitoring period.

[18] Data were collected at each transect using a mixed dipole-dipole array with a total sequence of 323 measurements collected; the same sequence was used for all transects. The sequence was selected to maximize coverage in the valley bottom with a minimum number of electrical current injections (to maximize temporal resolution of the data set). Data collection took ∼12 min per transect. The electrical resistivity distribution in the subsurface was assumed static during the collection for each transect (i.e., we did not account for changes between the first and last of the 323 measurements collected at each transect), and all data were assigned to the time at the midpoint of the data collection for a given transect.

[19] In an effort to maximize temporal resolution of ER data collection, all data were collected along individual transects; no between-transect data were collected. Background data were collected before the tracer injection began to characterize the distribution of background resistivity distribution. ER surveys were collected continuously for the first 12 h following the start of the tracer injection and for 12 h immediately following the end of the injection (i.e., when the rate of change of the EC in the hyporheic zone would be the greatest). ER surveys were collected every 2–4 h for the remaining times during the study (during both plateau and tailing conditions, when slower changes were expected). For this study, we limited our analysis to the first 120 h after the study began because that was the period during which data were collected for each of the four injections. To improve quality and estimate measurement error, a minimum of two measurements were stacked (i.e., averaged) for each resistance measurement. If the standard deviation for those measurements was greater than 2% of their average value, two additional data points were collected and included in the average. This additional collection occurred for 0.3%, 0.5%, 1.4%, and 2.5% of observations for injections 1–4, respectively. The final standard deviation of the measurements was recorded for each quadripole (defined here as any measurement consisting of two current and two potential electrodes). Reciprocal data and additional replicate measurements were not collected because of data collection time constraints (i.e., to maximize temporal resolution).

2.4.2. Data Inversion

[20] Electrical resistivity data inversion was completed using the research code R2 (v2.6, Generalized 2-D Inversion of Resistivity Data, available at http://www.es.lancs.ac.uk/people/amb/Freeware/freeware.htm). The algorithm, which is based on Occam's inversion, is described by *Binley and Kemna* [2005]. Individual data weights were applied, using the reciprocal of the standard deviation of stacked measurements. Inversion pixels dimensions were 25 cm in the horizontal and 20 cm in the vertical. Error model parameters were manually adjusted to yield a root-mean-square error (RMSE) with respect to the noise in the data as close to 1.00 as possible for the background inversion. Data collected during and after the tracer injection were inverted using the background model as a starting model. Thus, each time step was inverted independently [as by *Ward et al.*, 2010, 2012]. Time lapse-inversion [e.g., *LaBrecque and Yang*, 2001], or inversion of differences might provide some improvement in the results and should be considered for future studies. Inversion RMSE throughout the injection and monitoring period was used to determine time steps that failed to converge on a solution. For transects and time steps where inversion models did not converge due to high levels of noise in the data collected, the transect or time step was omitted from the analysis (transect 1 during injection 4 and transect 5 during injection 2 in our study).

2.4.3. Post-Processing

[21] The background (i.e., pretracer) resistivity image was subtracted from each of the images collected during and after the tracer study by calculating the percent change in resistivity for each pixel. Where salt-labeled stream water entered the subsurface, we expected resistivity to decrease compared to background. To quantify the hyporheic extent, we applied two filters. First, the diagonal of the resolution matrix (see, for example, *Binley and Kemna* [2005]) for each inversion was used to select only pixels where resolution was ≥ 0.01. This limits analysis to the pixels where the operator is able to uniquely determine at least 1% of a pixel value (i.e., 1% or more of a pixel's value is independent of adjacent pixels), based on the chosen measurement and inversion schemes. Next, we applied a threshold of a minimum decrease in electrical resistivity of 3% to parse meaningful changes due to tracer presence from error in the data collection and inversion. This threshold was selected to account for error in both data collection and inversion in a single parameter (after *Ward et al.* [2010]). The cross-sectional hyporheic area was calculated as the number of pixels meeting both filters multiplied by pixel area. This procedure was completed for each transect at all time steps. The calculated hyporheic area is sensitive to the thresholds set for both resolution and percent change. Selecting higher thresholds would result in smaller interpreted areas, and smaller thresholds in larger interpreted areas. While the absolute area of the hyporheic zone varies, relative trends in space and time are consistent across thresholds ranging from 2% to 4%.

[22] Finally, we compared the breakthrough curves observed in monitoring wells to pixel breakthrough curves (i.e., temporal trends in electrical resistivity at an individual pixel, based on results of geophysical inversion) in corresponding locations. Comparison of pixel breakthrough curves with observed point measurements has been successfully applied to characterize fluid flow and solute transport [e.g., *Binley et al.*, 1996; *Slater et al.*, 2000, 2002]. The purpose of our comparison is to demonstrate that the ER images are sensitive to the tracer in the subsurface. ER is based on the inversion of field measurements that are sensitive to 3-D volumes (though our inversion procedure assumes a 2-D distribution in resistivity extending in the third dimension); monitoring wells provide a spatially discrete measure of concentration. It is not expected that a perfect fit will be observed between the two because of a difference in the support volume for fluid conductivity (point-scale support volumes) and ER (electrical field-scale support volumes), but this comparison provides qualitative evidence of ER sensitivity to the tracer.

3. Results and Discussion

3.1. Hydrologic Changes During Base Flow Recession

[23] During base flow recession (early June to late August) in 2010 we conducted stream tracer studies at flows ranging from 35 to 4 L s^{-1} (Figure 2). Temporal trends in cross-valley and down-valley components of hydraulic gradients within the riparian zone for each triangular element are presented in Figure 3. A storm event early in the monitoring period created a large perturbation that relaxed by mid-June. The storm event caused some cross-valley gradients to increase in magnitude, although gradients turned both toward and away from the stream in different locations. After the catchment relaxed from the storm event, gradients for elements NH2, NH6, SA3, and TS1–5 turned away from the stream (i.e., toward the southwest valley boundary, negative in our convention), while those for NH1, NH3, NH7, and SA1–2 turned toward the stream (i.e., toward the northeast valley wall, positive in our convention). After the storm event, down-valley gradients for elements NH5, NH7, SA1–2, and TS3–4 decreased through the study period, while those for NH1–4, NH6, SA1, TS1–2, and TS5 increased through the remainder of the season. Overall, gradients in the valley floor turned toward the down-valley axis during the base flow recession season (i.e., steepening down-valley and/or lessening cross-valley magnitudes). Additional detailed analysis of the gradients throughout the study period is presented by *Voltz* [2011].

[24] The vertical hydraulic gradient was calculated at transects 3 (piezometer D4) and 5 (piezometer G4), where paired piezometer and in-stream water elevations were collected. At transect 3, the VHG was −0.619, −0.634, −0.701, and −0.679 m m^{-1} for injections 1–4, respectively. VHG at transect 5 was −0.436, −0.442, −0.454, and −0.450 m m^{-1} for injections 1–4, respectively. Little change in VHG (always downwelling at both locations) is noted under high and low base flow conditions, similar to observations reported by *Wondzell* [2006] at transect 3 (piezometer D4) in an earlier study.

3.2. Solute Tracer Studies

[25] The breakthrough curves for the four replicate tracer studies were logged at the upstream end of the study reach, below one mixing length (Figure 4). Background tracer concentration was subtracted from each observation set. Plateau EC values ranged from increases of 60–120 μS cm^{-1} during the injections. The plateau concentration of solute in the stream was highest during injection 2. This increased solute level did not change expected trends observed in the in-stream data (i.e., tailing behavior). Observations in monitoring wells during injection 2 reflected the increased tracer concentration during the plateau relative to other injections, but increased persistence of tracer presence in the well network was not observed (Figure 5).

[26] Injection rates were checked at intervals of 3–4 h to ensure a constant rate injection into the stream. Tracer arrival time at the study reach was fastest during the first injection, with the first arrival occurring within minutes of the injection start time, and slowed with decreasing flow rate, ultimately taking ∼20 min for first arrival during the final injection (Figure 4). Tailing behavior of the tracer was delayed between injections in a similar pattern to arrival time, with more prolonged tailing in each successive injection (Figure 4). This increased tailing suggests an increased influence of hyporheic exchange in retarding the transport of tracer through the study reach with decreasing flow.

3.3. Electrical Resistivity Imaging of Solute Tracer

[27] Both observed fluid EC and ER for the colocated wells and ER transects are presented in Figure 6. For monitoring wells, the 50-cm screened length intersected up to six pixels in the inversion images; for piezometers the screened section intersected a single pixel. Pixel resistivity trends are generally well correlated with monitoring well

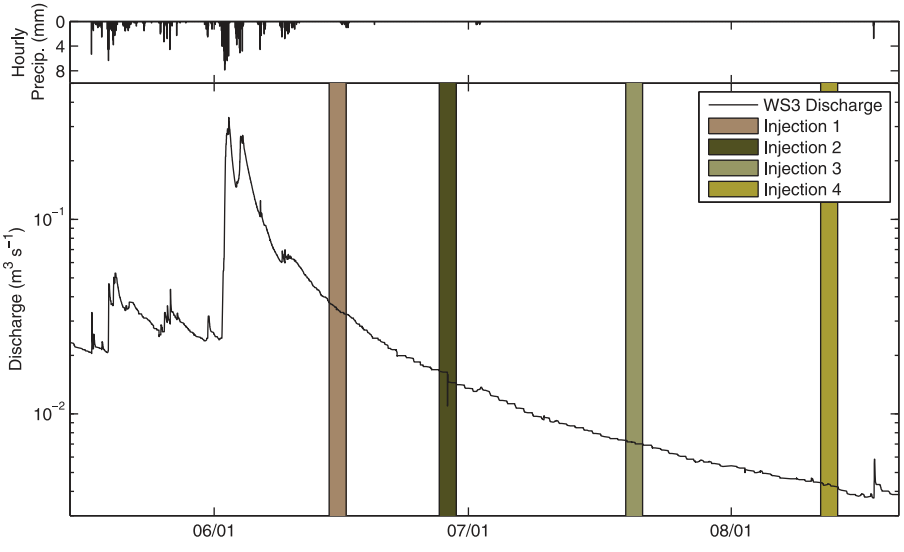

Figure 2. Flow and precipitation in WS3. Flow was gauged at a weir located ∼100 m downstream from each study reach. Precipitation records are from the Primary Meteorological Station at the H. J. Andrews Experimental Forest. Injection periods are shown as shaded bars. The discontinuity in the hydrograph during the second injection is due to the installation of a low-flow weir at the watershed outlet.

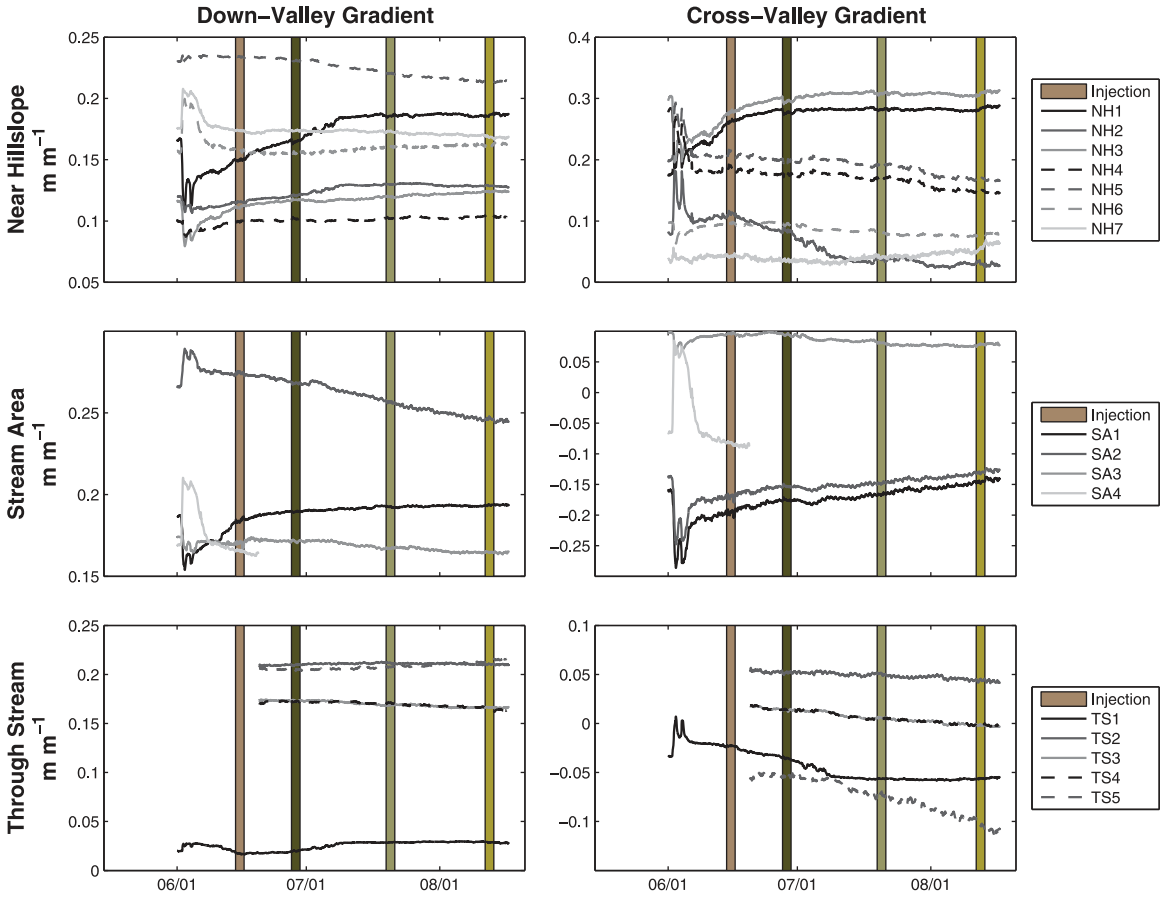

Figure 3. Down-valley gradient (i.e., gradient parallel to the valley bottom) and cross-valley gradient (i.e., gradient perpendicular to the valley bottom) for each element throughout the study period, in the left and right columns, respectively. Larger down-valley gradients indicate steeper down-valley components of hydraulic gradients; smaller values represent shallower down-valley gradients. For cross-valley gradient, positive values represent gradients toward the northeast valley wall; negative values represent gradients toward the southwest valley wall. Increased magnitude of cross-valley gradient indicates steeper gradients in that direction.

observations of EC. Decreases in predicted resistivity of the pixels are temporally aligned with the appearance and disappearance of tracer in the wells. No effort was made to optimize the resistivity models based on the well data; the comparison is presented only as evidence that the electrical geophysical models were sensitive to the solute tracer.

[28] Transect 1 was omitted from injection 4 due to a failure to converge in the inversion process, due also to noisy measurements. We suspect the falling water table and dryer conditions reduced the electrical contact between the electrode and soil matrix. For those locations where high-quality data were collected, mean stacking error in the ER data collected ranged from 0.08% to 0.46% for each transect during each injection. Mean RMSE for the inversions ranged from 1.00 to 1.10 for each transect during each injection. Excepting the omitted data, errors in both data collection and inversion remained low and relatively consistent throughout the study period.

[29] One additional complicating factor in interpreting 2-D ER images is the compression of temporally variable 3-D electrical fields into 2-D images with a single time step assigned. Temporally, we assume that the data collection time (~12 min) is much faster than the system is changing, and assume all data collected at a single transect is representative of a single time step (i.e., no temporal smearing of data). Spatially, the inversion scheme represents a single plane although the electrical observations are based on a fully 3-D field. Furthermore, this field is time-varying depending upon the distribution of the tracer in the subsurface. In our study, we ignore out-of-plane effects of this inversion scheme but note that the implication of this assumption is that we may sense upstream tracer before it arrives at the transect (or, similarly, downstream tracer after it has passed by the transect itself). Thus, we expect some degree of temporal smearing in our data.

3.4. Changes in Peak Hyporheic Extent and Timing Through the Seasonal Base Flow Recession Period

3.4.1. Hyporheic Dynamics Interpreted From ER Images

[30] ER images of solute in the subsurface are presented at 24, 48, and 72 h after the start of the injection (Figures 7A, 7B, and 7C, respectively). After 24 h tracer appears in the alluvial deposit adjacent to the stream in transects 1–3,

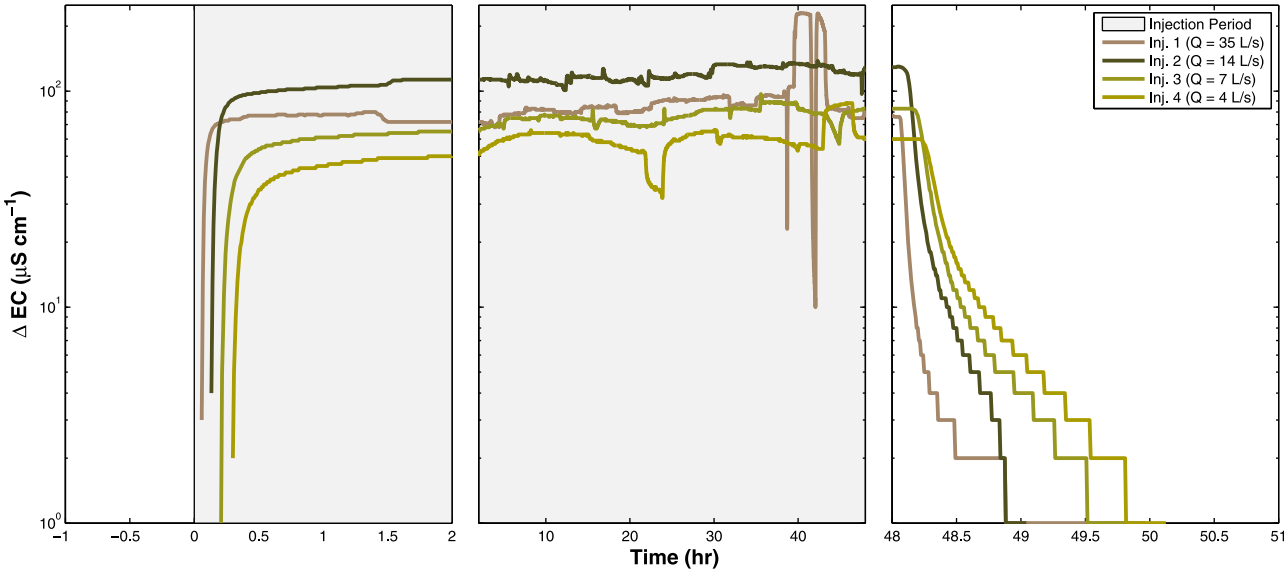

Figure 4. Breakthrough curves at the upstream end of the study reach in WS3, as the change in observed electrical conductivity (EC) of the surface water (a surrogate for the concentration of the sodium-chloride tracer) in log-space. The three panels provide increased resolution on the rising (left panel) and tailing (right panel), while the center panel shows the plateau conditions during a majority of the injection. The injections occurred from times 0–48 h. During tracer injection 1 the injection rate approximately doubled after about 39 h of injection (at ∼03:00). This change was discovered at ∼06:00 and the injection flow rate was reset to its initial rate. Arrival time at the study reach was increasingly later as streamflow decreased during the season. Studies during lower flow conditions show increased tailing at late times, suggesting increased transient storage between the injection point and study reach.

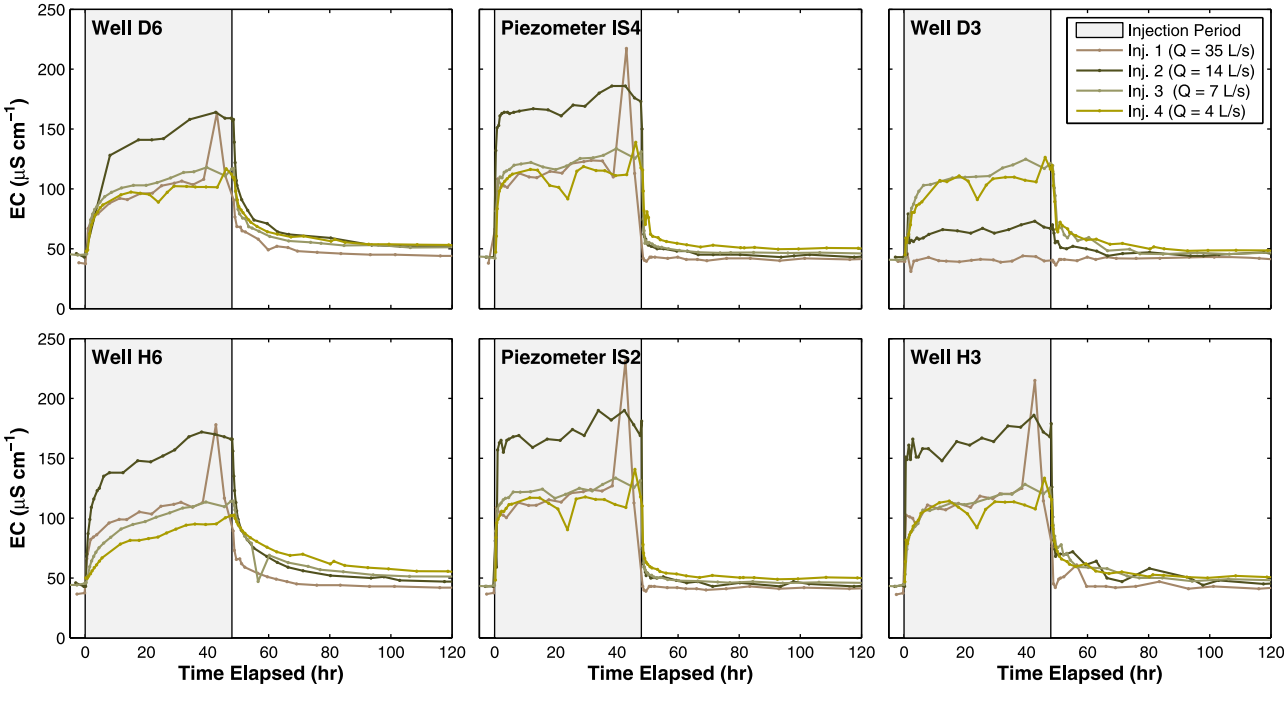

Figure 5. Representative observations from the monitoring well network, representing observations on the southwest bank (left column), streambed piezometers (center column), and northeast bank (right column) in less confined (i.e., downstream, top row) and confined (i.e., upstream, bottom row) locations. Increased plateau tracer concentration during injection 2 was observed in the piezometers and southwest bank monitoring wells. Transport to wells on the northeast bank increased during lower flow conditions.

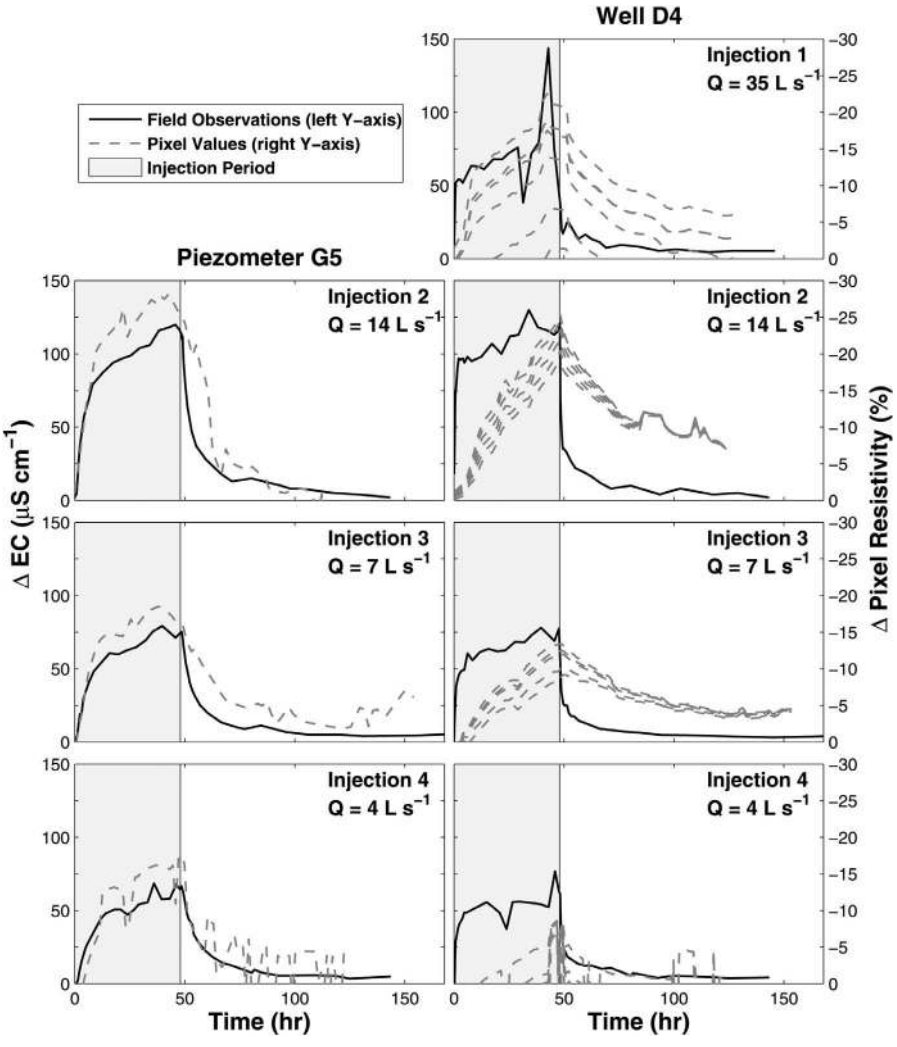

Figure 6. Examples of observed monitoring well tracer concentration (as change in electrical conductivity) and change in pixel resistivity for piezometer G5 (left column) and well D4 (right column) during each injection. Multiple lines are shown where the well screen intersects multiple pixels in the inversion. Each row corresponds to one of the four constant-rate injections. Tracer presence in wells is temporally correlated with the observation of tracer in the electrical resistivity models, demonstrating that the ER models are sensitive to the solute tracer. Because concentration is a point measurement and pixel resistivity is based on 2-D inversion of a 3-D field measurement, perfect agreement is not expected. However, results demonstrate conclusively that the geophysical inversion is sensitive to the tracer.

although in a relatively small cross-section. The hyporheic zone appears to pinch out at transect 3. Downstream, a large hyporheic zone, as evidenced by tracer presence in the subsurface, is observed in transects 4–5 after 24 h (Figure 7A). When the injection is stopped after 48 h (Figure 7B), similar spatial trends are observed, though the hyporheic zone is spatially larger than observations after 24h at all cross-sections. After 72 h (24 h after the solute injection ended), the tracer has been flushed from the suite of temporally shorter flow paths, although a substantial hyporheic zone is still observed, suggesting longer spatial and temporal scale flow paths are present (Figure 7C).

[31] The peak change in pixel resistivity during each injection (Figure 8) provides a time-independent analysis, which allows for comparison of solute presence or absence in the subsurface between injections without the complicating factor of arrival time at a given location. For transects 1–3 (steeper, confined valley), the hyporheic area appears largest for the highest flow rate conditions. At transects 4 and 5 (wider, less-confined valley) the spatially largest hyporheic zones are observed during injection 2, with smaller plumes during injections 1, 3, and 4 (Figure 9). These results oppose the widely held conceptual model that increased head gradients toward the stream constrict hyporheic flow path networks [e.g., *Hakenkamp et al.*, 1993; *Hynes*, 1983; *Meyer et al.*, 1988; *Palmer*, 1993; *Vervier et al.*, 1992; *White*, 1993]. Furthermore, these results agree with observations by *Harvey et al.* [1996] that found a larger hyporheic extent during lower flow conditions.

[32] Both spatial patterns of exchange and the late-time presence of solute along hyporheic flow paths (hereafter "persistence") can be assessed qualitatively using time-lapse

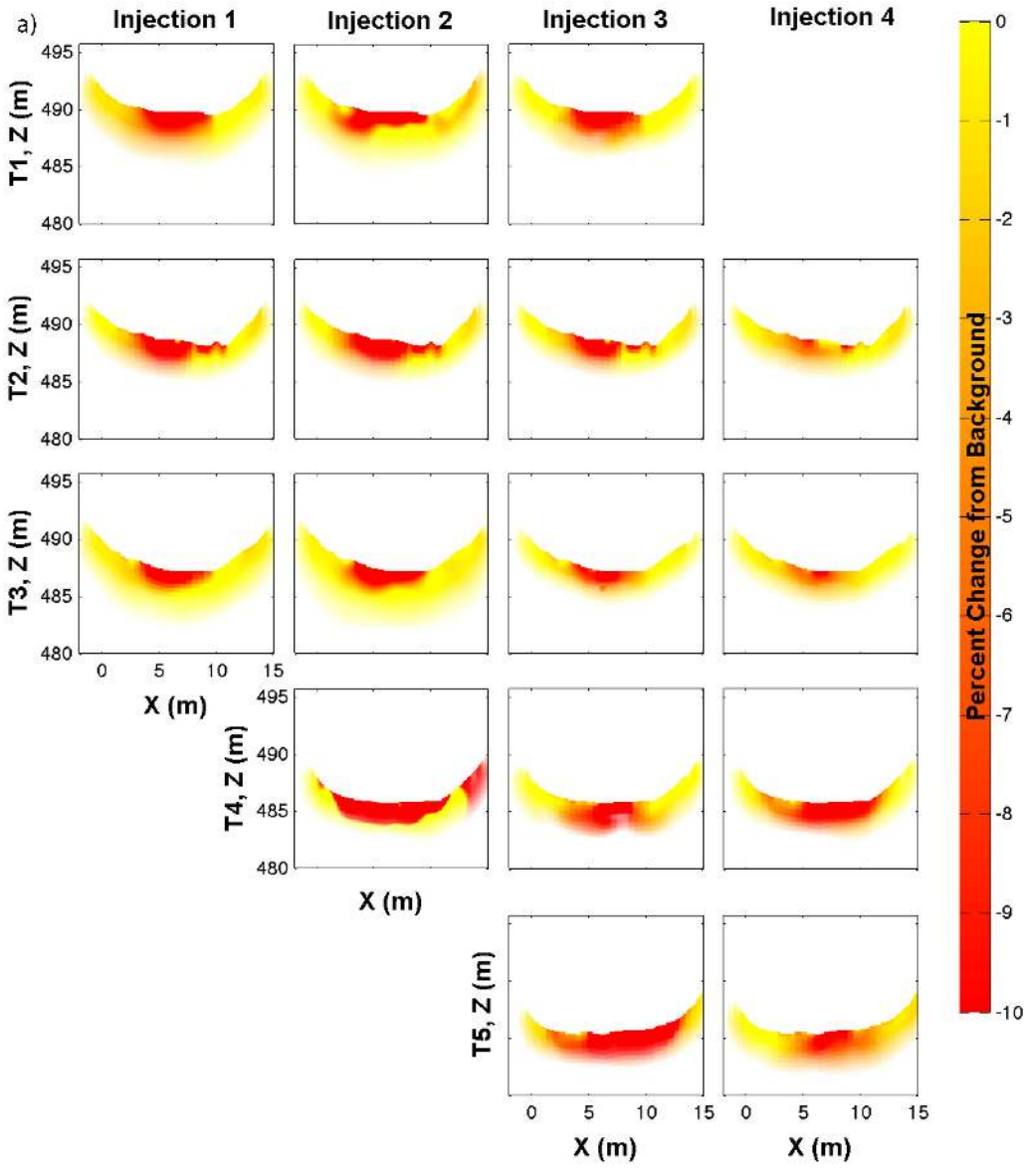

Figure 7. (a) Visualization of hyporheic extent 24 h after the start of each injection. Color relates to the observed drop in pixel resistivity; opacity is based on resolution matrices with less certain data plotted as transparent (pixels with $\log_{10}$[resolution] < -2 are shown in white). Hyporheic location and extent are spatially consistent for transects 1, 2, and 4 across all injections. Hyporheic extent at transects 3 and 5 appears to decrease with decreasing flow (peak hyporheic extent and its timing are summarized in Figure 9). Plateau concentration during each injection ranged from 60 to 120 μS cm^{-1}, with the highest plateau during injection 2 and the lowest during injection 4. (b) After 48 h, hyporheic areas are larger than those at 24 h elapsed. Spatial differences are apparent in transects 2–5. See Figure 10 for areas through time for each transect and injection. (c) After 72 h, hyporheic flow paths are still labeled with solute tracer, particularly in transects l–4. At this time the stream returned to background concentration for all injections (based on in-stream logging of electrical conductivity). Electrical resistivity imaging is able to characterize flow paths that are beyond the window of detection for traditional solute tracer studies. The in-stream plateau achieved was highest during injection 2, which delivered increased solute mass along hyporheic flow paths, which may contribute to the highly persistent flow paths observed during that injection.

images of the subsurface, and more quantitatively through late-time behavior observed in the plots of hyporheic area through time (Figure 10). We emphasize here that the interpreted areas are sensitive to the thresholds chosen [*Ward et al.*, 2010]. Temporal trends in a hyporheic area are generally similar between injections for transects l–3 (steeper, confined valley), while transects 4–5 (flatter, less-confined valley) exhibit greater variability (Figures 9, 10).

[33] The increased persistence observed in ER data during injection 2 is anomalous relative to trends that appear

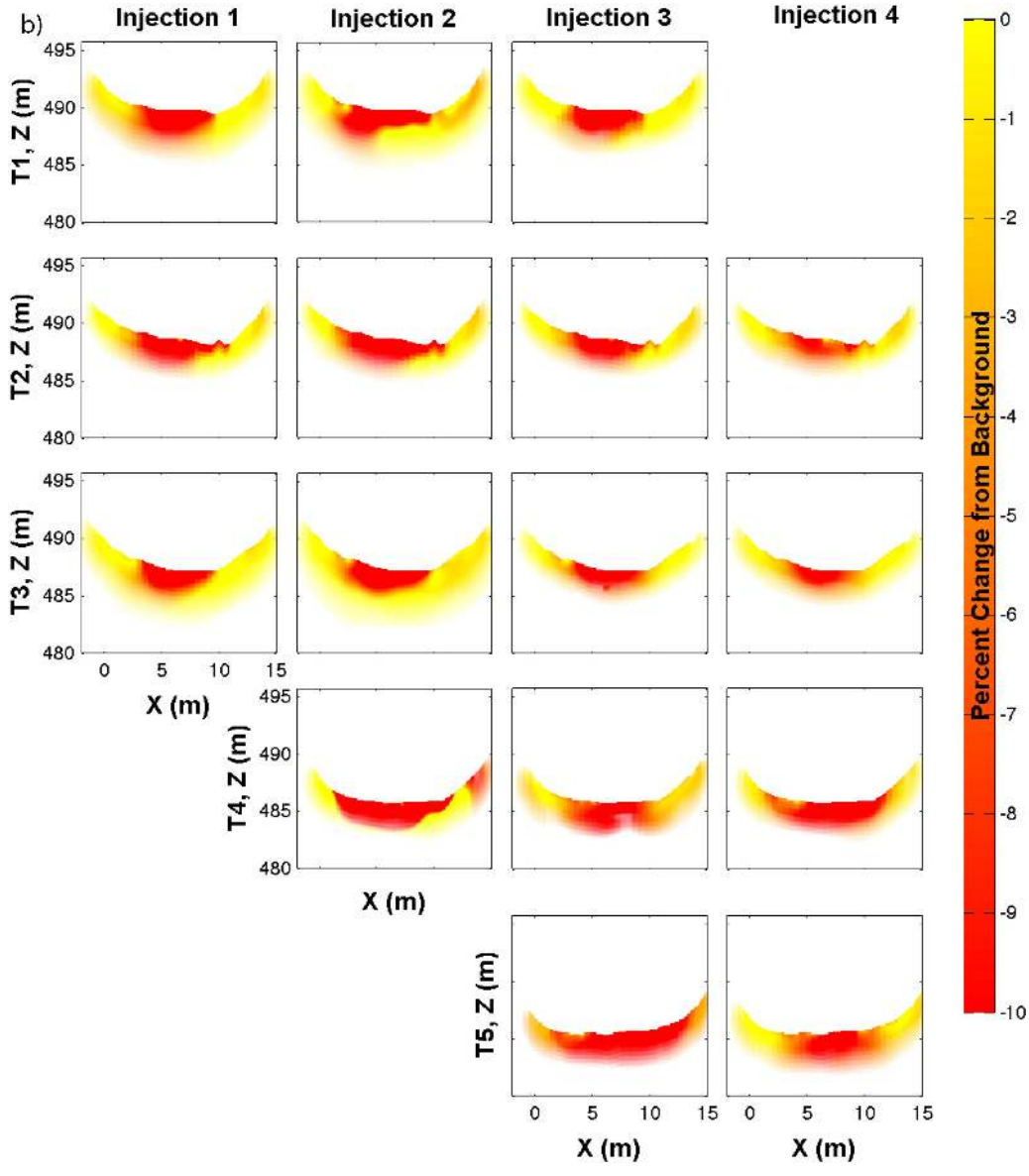

Figure 7. (continued)

for the other three injections. Discrete monitoring-well observations do not suggest increased persistence due to the higher in-stream plateau during injection 2 (Figure 5). We attribute the increased persistence during injection 2 to an increased concentration of tracer at plateau during the injection. We posit exchange of the saline tracer between mobile pore water and less mobile pore water (i.e., water bound to sediment grains, in dead-end pore spaces, etc.), due to the increased concentration gradient between the mobile pore water and less mobile hyporheic water. This would explain the increased persistence of tracer observed in the ER data despite the monitoring wells showing no evidence of increased tracer persistence. Ultimately, the increased persistence is attributed to the higher plateau concentration of the solute injection; we cannot definitively say this was a function of the hydrologic conditions. Observations of persistence based on ER data are sensitive to experimental design, a limitation that should be considered in future experimental design and interpretation of results.

[34] The 2-D information provided by the ER images allows assessment of both vertical and lateral constraint in the subsurface, whereas previous studies have only been able to assess this control at the broad, valley scale. In the steeper, confined section of the valley (transects 1–3), the lateral extent of tracer penetration into the aquifer is relatively consistent under all flow conditions. Vertical penetration is decreased for injections with lower flow rates. It is likely that lateral confinement limits the tracer along the northeast valley boundary ($X = 10$ and larger). Vertical confinement limits the hyporheic extent in higher-flow conditions for these transects (area change in the vertical dimension indicates confinement is not the control). In contrast, the flatter (i.e., lower down-valley gradient of the land surface) and less-confined lower portion of the study reach (transects 4–5) exhibits lateral penetration that is more sensitive to cross-valley gradients. The changing lateral extent of the hyporheic zone in transect 4 shows the cross-valley control in this section of the study reach.

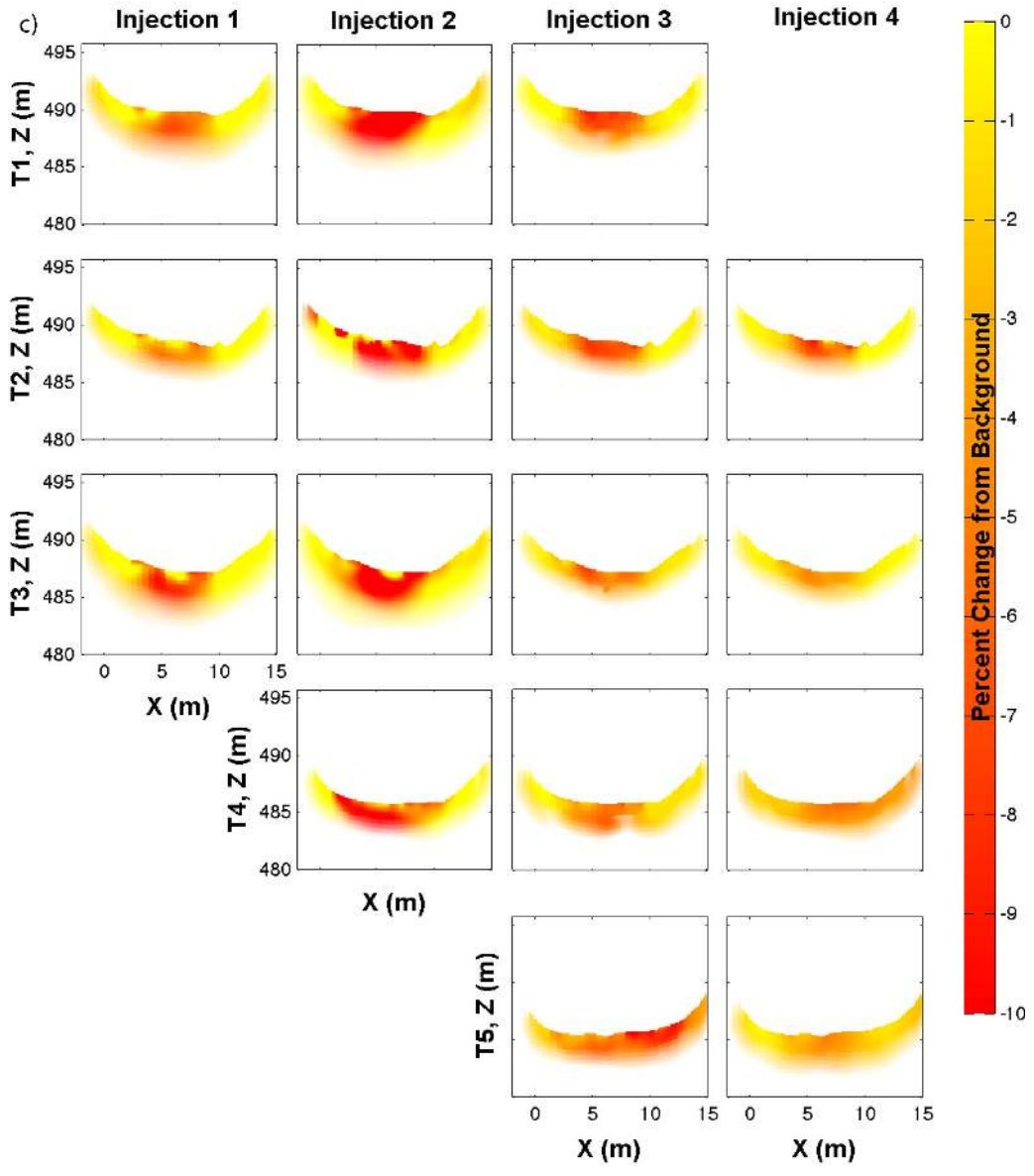

Figure 7. (continued)

Consistent vertical penetration suggests that vertical confinement is not limiting at transects 4–5.

3.4.2. Spatial and Temporal Trends in Peak Hyporheic Extent

[35] Our findings show that hyporheic extent, as interpreted from 48-h stream tracer injection studies, increases with decreasing stream discharge when fitting a trend to all data collected (Figure 11A). Analysis of individual transects, however, reveals this trend is not robust. Increasing hyporheic extent with decreasing flow rate is only apparent for transect 4 (Figure 9). At all other transects the largest hyporheic extent was observed during intermediate flow conditions (injections 2 and 3), with smaller extent observed during both the highest and lowest flow conditions. We hypothesize behavior at transect 4 is explained by its location immediately downstream from a bedrock "pinch point" in the valley; downwelling at this location is likely to occur, and may be mediated by 3-D hydraulic gradients. This unique morphological location, in combination with changing hydraulic gradients, likely leads to this behavior, while other transects are in locations that are less dominated by hydraulic gradients. In-stream flow rate is not sufficient to explain the observed peak hyporheic extent in our study. Because solute tracer was observed in all wells in the monitoring network during all studies, these data cannot be used to refine our quantification of hyporheic extent.

[36] Spatial trends in peak hyporheic extent vary with in-stream flow rate, though no universal trend is present (Figure 9A). Transects in the upper (steeper, confined valley; transects 1–3) and lower (flatter, less-confined valley; transects 4–5) segments showed little difference in peak hyporheic extent during injection 2. During injections 3 and 4, however, the transects in the less-confined reach had hyporheic extents that were larger than those in the

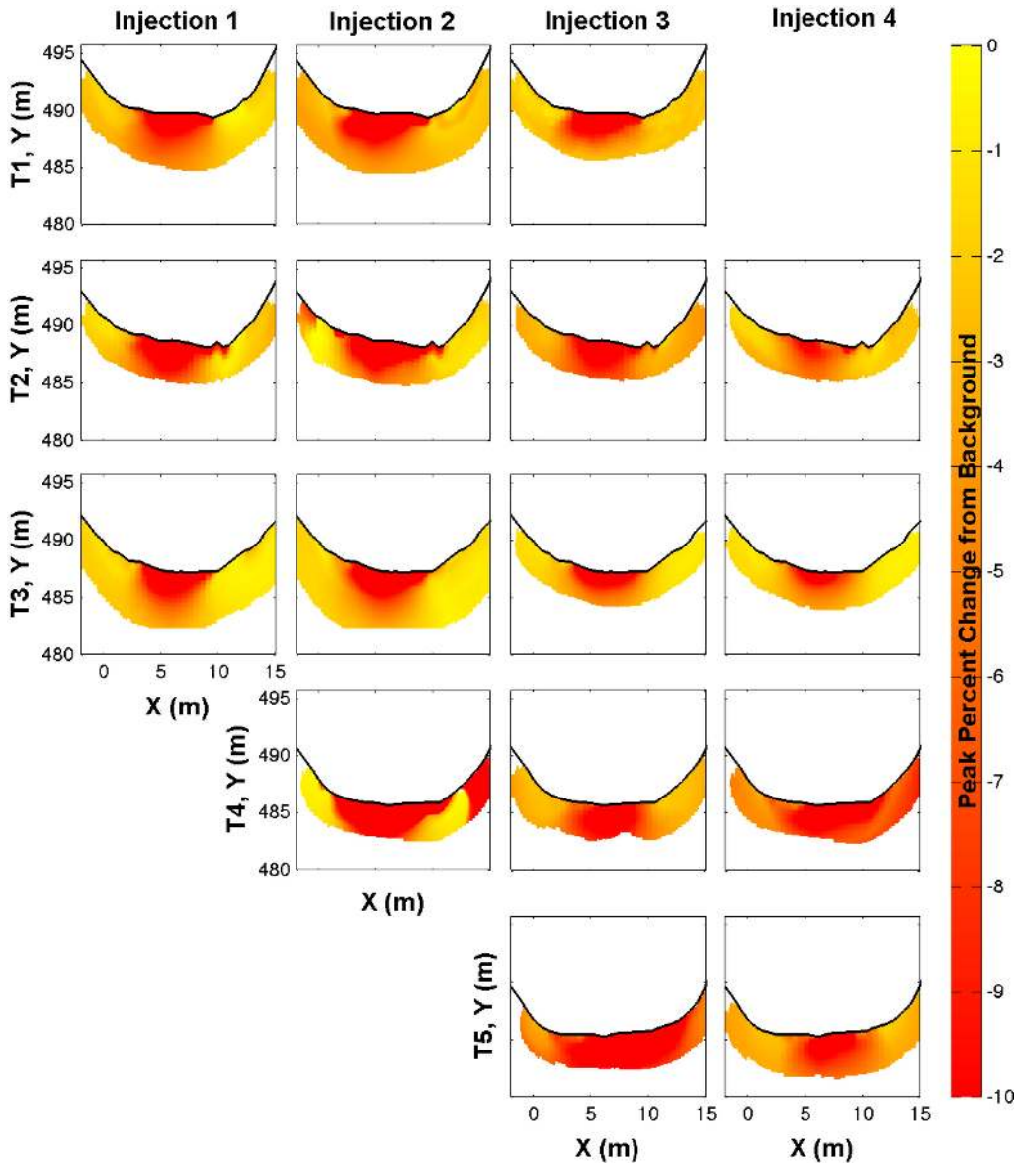

Figure 8. Peak changes in pixel resistivity observed during the tracer study. The distribution of the peak change in pixel resistivity provides a time-integrated view of the distribution of solute tracer in the subsurface. Opacity is not based on values of pixel resolution (in contrast to images shown in Figure 7).

confined reach. During the lowest flow experiment (injection 4) this difference is most apparent. Larger peak extent in downstream transects suggests an increased hyporheic exchange in these locations.

3.4.3. Spatial and Temporal Trends in Time to Peak Hyporheic Extent

[37] Time elapsed between the start of the tracer injection and observation of peak hyporheic extent is summarized in Figure 9B. Peak arrival time is generally later during lower flow conditions for transects 4–5. No clear trend with in-stream flow rate is observed for transects 1–3. During injections 1–3, no clear trend is present with respect to the spatial pattern in peak arrival time. For injection 4, peak arrival is substantially later at transects in less-confined locations (transects 4–5).

[38] We expected that the peak arrival time would be later during lower flow conditions (when we expected reduced down-valley gradients to more slowly transport solute along hyporheic flow paths); we did not find evidence to support this at all transects, though it appears to hold at transects 4 and 5. We expected later peak arrivals would be observed at downstream transects (owing to subsurface transport along flow paths from upstream to downstream transects, from transects 1–3, for example). Again, we did not find evidence supporting this expectation. While the late-time presence of solute in downstream transects may be due to subsurface transport from upstream locations, this does not appear to be the primary mechanism for solute to arrive at any given transect. Down-valley pore water velocity in the upper and lower reaches can be calculated using Darcy's law. Approximating hydraulic gradient

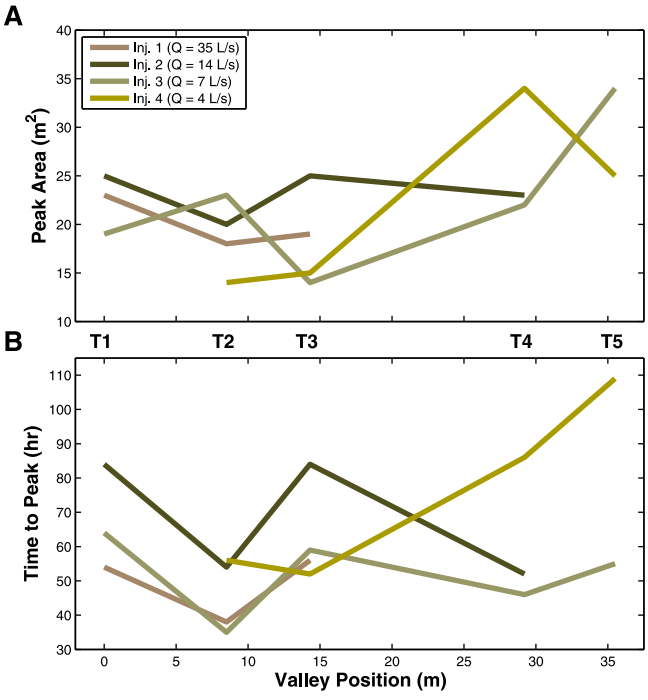

Figure 9. Summary of peak hyporheic extent and its timing for all transects and injections. The location of each geophysical transect along the valley bottom is identified as T1, T2, etc. (A) Spatially, larger hyporheic zones were observed at the down-valley end of the reach for a given flow condition, particularly for the third and fourth injections (the lower-flow conditions observed). No consistent relationship between peak area and either location or hydrologic condition is apparent in the data. (B) Peak hyporheic area at T5 occurred later in time than those observed at upstream (more constrained) locations during the lowest flow conditions. No consistent relationship between peak arrival time and either location or flow condition is apparent in the data.

and the subreach scale with topographic gradient (16% and 6% for upper and lower reaches, respectively), using estimates of 5×10^{-5} m s^{-1} for hydraulic conductivity (after *Ward et al.* [2011], using values within the range reported by *Wondzell et al.* [2009]), and estimating porosity at 30% (after *Ward et al.* [2011]. Down-valley transport in the subsurface pores ranges from 1.0 to 2.7×10^{-5} m s^{-1}. Given these velocities, we conclude that advection from the stream channel to the subsurface along hyporheic flow paths, rather than subsurface transport from up-valley along much larger spatial-scale and longer temporal scale flow paths, may be the dominant process.

3.5. Valley-Bottom-Averaged Hydraulic Gradients and Hyporheic Extent

3.5.1. Down-Valley Hydraulic Gradients

[39] Hyporheic area as a function of the valley-bottom-averaged down-valley gradient is plotted in Figure 11C. Overall trends show an increasing peak hyporheic area based on the ER with an decreasing down-valley hydraulic gradient. Individual transects, however, exhibit more complex behavior. In the upper reach (i.e., transects 1–3, steeper and more confined), an increasingly steep down-valley gradient was weakly related to decreasing hyporheic extent, though individual behavior about this relationship is widely varied. For transect 4 (in the flatter and wider section of the study reach), an increasingly steep down-valley gradient trended with increasing hyporheic extent, while transect 5 (the next transect downstream) showed the opposite behavior. Transect 4 is the first transect downstream from an apparent "pinch point" in the hyporheic zones that causes upwelling of hyporheic flow paths. Downwelling is expected at transect 5 because an increased subsurface capacity to transport water down-valley is present; steeper down-valley hydraulic gradients more rapidly drive flow into the subsurface yielding larger observed hyporheic areas.

3.5.2. Cross-Valley Hydraulic Gradients

[40] Overall trends show an increasing peak hyporheic extent with increasingly positive valley-bottom-averaged cross-valley gradients (i.e., a larger extent when gradients from the hillslope to the stream are larger; Figure 11D). This relationship holds for transects 1–3 (in the steeper, confined section of the study reach) and at transect 5. As with the down-valley gradient, behavior at transect 4 is anomalous, showing a decreasing hyporheic area with increasingly strong cross-valley hydraulic gradients toward the stream. The behavior at transect 4 fits the general conceptual model of cross-valley hydraulic gradients compressing hyporheic networks, while the behavior at transects 1–3 and 5 is in opposition to this model. The behavior in upstream transects suggests that cross-valley hydraulic gradients are not the limiting factor in a hyporheic extent. Rather, it is likely that confinement due to bedrock limits hyporheic exchange in these locations, and influences the cross-valley hydraulic gradients. We hypothesize in this case that it is not the gradients from the hillslope to the valley bottom that control exchange, but another process or factor (e.g., subsurface confinement, variability in the hydraulic conductivity field, riparian water demand, etc.).

3.5.3. Vertical Hydraulic Gradients

[41] Hyporheic extent shows a positive relationship with a decreasing VHG magnitude at transect 3 (i.e., stronger gradients away from the stream trend with smaller peak hyporheic areas; Figure 11B). At transect 4, VHG was nearly constant across the observed flow conditions, and we find no trend between the VHG and peak hyporheic area at this location. In contrast to our conceptual model of increased hyporheic extent due to losing conditions, we find increasing VHG trends with a decreasing hyporheic extent at transect 3.

[42] Results at transect 3 oppose the conceptual model of compressed hyporheic zones under strong gaining conditions that has been reported in both numerical [e.g., *Boano et al.*, 2008; *Cardenas and Wilson*, 2007b; *D'Angelo et al.*, 1993] and field studies [e.g., *Harvey and Bencala*, 1993; *Storey et al.*, 2003; *Williams*, 1993; *Wondzell and Swanson*, 1996; *Wroblicky et al.*, 1998]. While increasingly strong hydraulic gradients away from the stream may expand hyporheic zones (or conversely, increasing hydraulic gradients toward the stream compress hyporheic zones), our results do not indicate hyporheic expansion with

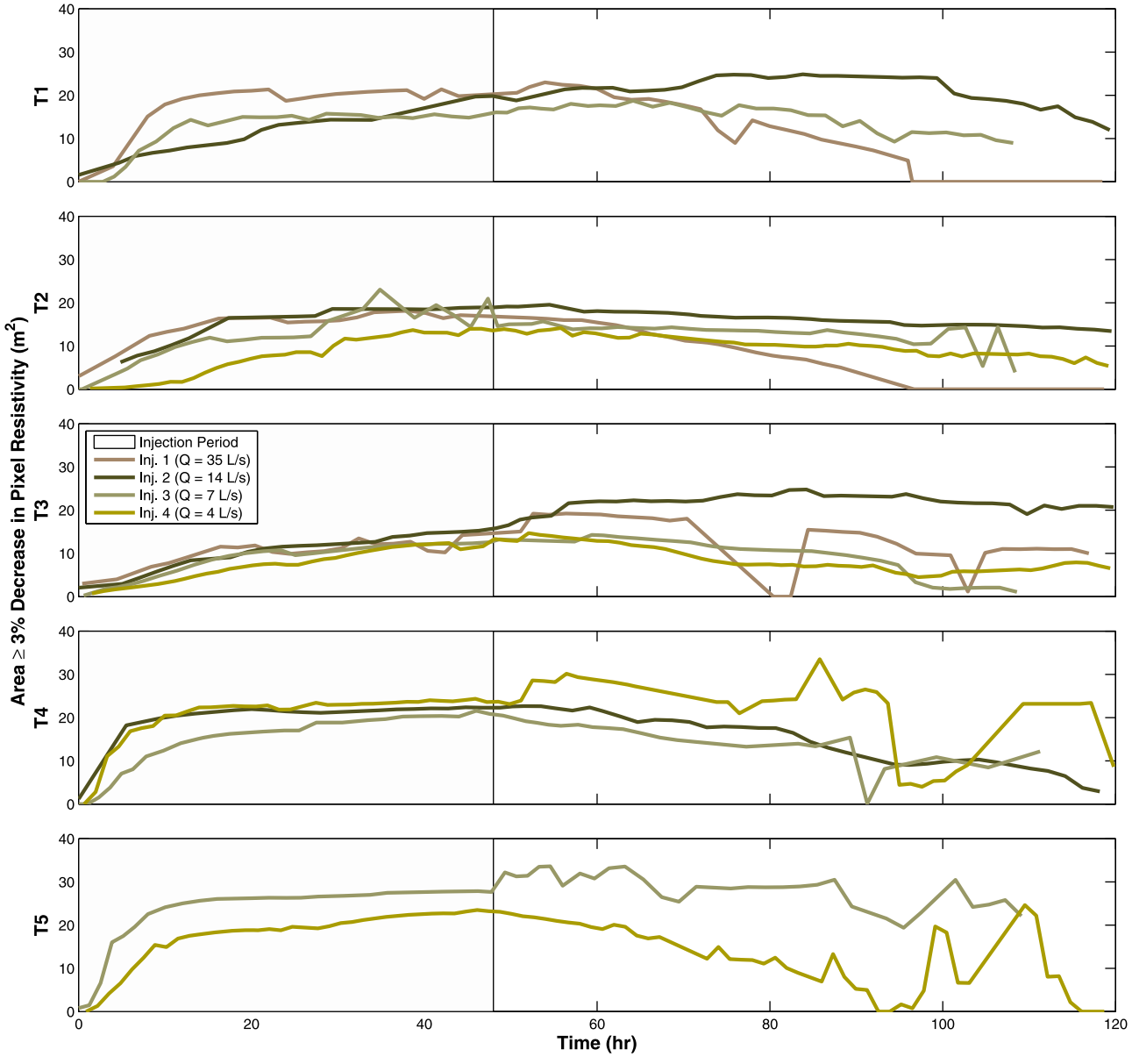

Figure 10. Temporal trends in hyporheic area (minimum 3% decrease in resistivity) based on electrical resistivity images. Peak hyporheic area and temporal trends for transects 1–3 (in the steeper, more confined section of the study reach) are generally constant between different flow conditions. In the flatter, wider valley segment we observed larger peak areas and later peak arrivals at transect 4, though these trends were not apparent at transect 5. Results suggest bedrock confinement may limit hyporheic extent in transects 1–3, while the less-constrained transects 4–5 are more strongly controlled by hydraulic gradients in the valley bottom.

increasingly losing VHG at the site of the observations. We do not refute the findings of the field and numerical studies above, rather we find our observations of VHG and hyporheic extent at T3 are not measuring the same response. It is likely that the observed extent at T3 would be more appropriately related to VHG observed some distance upstream of the ER transect (i.e., the plane of observation for the ER data is sensitive to flow paths that originated at unknown upstream locations, while the VHG is measured at the transect itself). This example underscores the need for observation of the flow field in three-dimensions in order to draw conclusions about solute transport behavior at any given location; the observed VHG is not at the location where the flow paths intersecting T3 leave the stream channel.

3.6. High-Resolution Hydraulic Gradients and Hyporheic Extent

[43] Based on the analysis of valley bottom average cross- and down-valley hydraulic gradients and hyporheic area, which showed overall trends with a high degree of variability for individual transects, cross- and down-valley hydraulic gradients at each were plotted against the observed peak hyporheic area at each transect. We calculated the

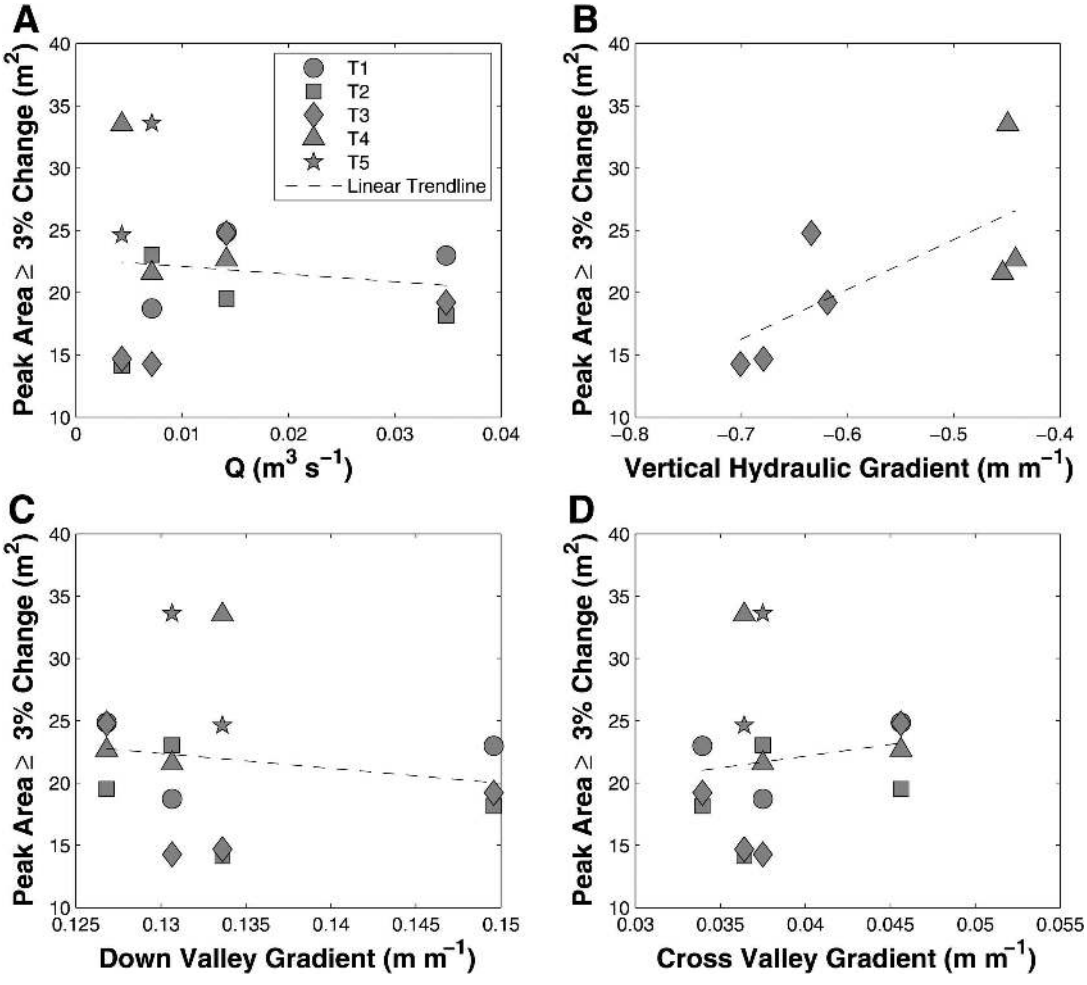

Figure 11. Peak hyporheic area as a function of (A) streamflow, (B) vertical hydraulic gradient, (C) valley-bottom-averaged down-valley gradient, and (D) valley-bottom averaged cross-valley gradient. Overall trends (dashed lines) show the relationship between peak area and flow is slightly negative. Hyporheic extent is negatively related to down-valley gradient (i.e., increasingly steep down-valley gradients generate smaller hyporheic zones) and positively related to increasing cross-valley gradient (i.e., increasingly strong gradients toward the stream). Increasingly strong vertical hydraulic gradients away from the stream are related to the smaller peak hyporheic area, in opposition to the conceptual model of "compressed" hyporheic zones with stronger gradients toward the stream. In all cases, data are highly variable about the overall relationships, and these relationships break down when considering individual transects.

slope of linear trend lines for each element-transect pairing, considering both down-valley (Table 1) and cross-valley hydraulic gradients (Table 2). We compare every triangular element with every peak hyporheic area observed because the flow paths present at each ER transect are a complex function of the hydraulic gradients in the entire valley bottom, not only those that intersect the transect itself. This analysis considers hydraulic gradients at a more local scale than the valley-bottom averages presented in Figures 10C and 10D. We do not posit that linear relationships are necessarily expected to provide the best fit; these data are presented only to consider general positive and negative relationships between hydraulic gradients and areas. The data in Tables 1 and 2 demonstrates the variability in the relationships between cross- and down-valley hydraulic gradients (even at a highly resolved spatial level) and hyporheic extent. As reported, variability can be inferred from both the presence of positive and negative relationships for individual elements or transects, and from the magnitudes of slopes (ranging across five orders of magnitude). These tables demonstrate that local hydraulic gradients are not the only control on hyporheic extent. As such, these data should be interpreted only as a binary indication (i.e., positive or negative) of the relationship between cross- and down-valley hydraulic gradients with hyporheic area.

3.6.1. Down-Valley Hydraulic Gradients

[44] In the lower-gradient and less-constrained valley section, increasing near-hillslope down-valley hydraulic gradients trend with decreasing areas (NH1–4); in the steeper and more constrained upper reach, increasing near-hillslope down-valley hydraulic gradients trend with increasing

Table 1. Linear Regression Slopes for Triangular Element Down-Valley Gradient Versus Area Relationships[a]

	Electrical Resistivity Transects				
Near Hillslope	1	2	3	4	5
NH1	−1.36	−0.04	−1.98	**5.58**	−4.18
NH2	−3.49	**0.53**	−5.32	**14.24**	−8.48
NH3	−2.82	−1.31	−4.17	**16.74**	−22.39
NH4	−5.68	−1.54	−9.12	**86.61**	−117.64
NH5	**3.69**	**1.03**	**4.29**	−7.75	**7.71**
NH6	−10.41	−1.66	−15.45	**19.46**	−14.92
NH7	**161.83**	**10.55**	**9.08**	−8.08	**20.18**
SA1	−3.10	−0.18	−4.69	**32.95**	−29.75
SA2	**2.58**	**0.89**	**2.85**	−5.52	**6.18**
SA3	**12.87**	**3.91**	**13.38**	−19.19	**19.73**
TS1	−4.83	−0.13	−7.06	**13.48**	−9.57
TS2	−32.17	**24.86**	−49.17	**64.33**	−10.15
TS3	**14.77**	**6.27**	**17.52**	−19.26	**19.41**
TS4	**54.69**	**8.90**	**8.05**	−7.39	**15.20**
TS5	−15.75	−5.95	−8.45	**8.57**	−12.41

[a]Linear regression analysis of gradient-area relationships provides insight into general patterns. Boldface entries (positive values) indicate relationships where steeper down-valley gradients are related to increased hyporheic area. Patterns show that steeper down-valley gradients are related to decreasing hyporheic extent for near-hillslope (NH) elements, and related to increasing hyporheic area for observations in both stream-adjacent (SA) and through-stream (TS) elements. Linear regression slopes for down-valley hydraulic gradient versus peak hyporheic extent (all values times 10^2).

hyporheic extent (NH5 and 7, in particular). Steeper down-valley hydraulic gradients trend with increasing hyporheic area for stream-adjacent triangular elements (SA), and no clear relationship is present in the through-stream (TS) elements. In all down-valley gradient analyses, transect 4 is anomalous in its behavior compared to the other transects.

Table 2. Linear Regression Slopes for Triangular Element Cross-Valley Gradient Versus Area Relationships[a]

	Electrical Resistivity Transects				
Near Hillslope	1	2	3	4	5
NH1	−1.42	−0.26	−2.19	**16.05**	−17.26
NH2	**0.68**	**0.09**	**0.94**	−2.27	**1.89**
NH3	−1.33	−0.06	−1.96	**9.18**	−7.56
NH4	**1.16**	**0.97**	**1.46**	−2.74	**5.23**
NH5	**1.16**	**0.84**	**1.39**	−2.72	**4.76**
NH6	**3.11**	**0.38**	**4.28**	−7.62	**6.02**
NH7	−3.59	−3.07	−3.38	**3.21**	−5.70
SA1	−1.11	−0.66	−1.37	**3.16**	−4.78
SA2	−1.30	−0.96	−1.67	**3.61**	−6.23
SA3	**3.09**	**0.39**	**4.25**	−7.53	**5.96**
TS1	**1.49**	−0.02	**2.19**	−5.77	**4.05**
TS2	**32.73**	8.88	**9.81**	−9.47	**16.47**
TS3	**7.50**	3.34	**7.01**	−7.50	**8.63**
TS4	**6.84**	2.99	**7.47**	−8.13	**8.61**
TS5	**3.16**	1.19	**1.68**	−1.70	**2.47**

[a]Linear regression analysis of gradient-area relationships provides insight into general patterns. Boldface entries (positive values) indicate relationships where steeper cross-valley gradients are related to increased hyporheic area. Steeper cross-valley gradient toward the stream is associated with increased hyporheic area for both NH and TS elements, and with decreased hyporheic area for SA elements (with anomalous behavior at transect 5 observed in all cases). There is variability within these general patters for both down-valley and cross-valley gradients. Linear regression slopes for cross-valley hydraulic gradient versus peak hyporheic extent (all values times 10^2).

[45] We hypothesized that the steepest down-valley hydraulic gradients would drive the largest hyporheic exchange, because such gradients would create the largest capacity for down-valley subsurface flows. This hypothesis is neither confirmed nor rejected based on our observations. In near-hillslope, stream-adjacent, and through-stream elements, we found both positive and negative relationships between the hyporheic area and down-valley hydraulic gradient. While steeper down-valley hydraulic gradients should increase down-valley transport capacity, it is possible that the added water that actually flows along these flow paths originates at the hillslopes rather than the stream channel, resulting in little effect on hyporheic exchange. In all elements, transect 4 is anomalous in behavior compared to a majority of the other transects. This behavior suggests that down-valley hydraulic gradients are not a primary control at this location; a hydrogeologic setting may be the primary control. We believe the physical location of transect 4 at a valley transition (between a steeper, confined upstream valley and flatter, less-confined downstream valley) overshadows any behavior related to flow rates or down-valley hydraulic gradients.

3.6.2. Cross-Valley Hydraulic Gradients

[46] Positive cross-valley hydraulic gradients in our study are directed toward the northeast valley boundary and negative cross-valley hydraulic gradients toward the southwest valley boundary (Table 2). NH2 and NH4–6 behave in opposition to the conceptual model of stronger cross-valley hydraulic gradients toward the stream channel compressing hyporheic flow path networks (i.e., a negative relationship between the cross-valley hydraulic gradient and a peak hyporheic extent). NH1, NH3, and NH7 fit our conceptual model of a negative relationship. SA1–2 fit our conceptual model, while SA3 does not. All TS elements show increasing hyporheic extent with increasingly positive cross-valley hydraulic gradients for all transects except transect 5 (see explanation above in section 3.6.1 regarding the physical setting as the primary control in this location). Because TS elements are informed by data from both banks, it is difficult to interpret these changes as increasingly toward or away from the stream.

[47] We hypothesized that the size of the hyporheic zone would expand during the base flow recession due to falling cross-valley hydraulic gradients from the hillslopes toward the stream. Our study found falling cross-valley hydraulic gradients toward the stream occurred with increased hyporheic area for some elements, but there was no consistent trend. The expected relationship was present in the elements closer to the riparian valley-hillslope transition (i.e., NH1, NH3, NH7, SA1–2), while elements closer to the hillslope show the opposite relationship (i.e., NH2–4, NH6). The results of this study show that hyporheic compression by cross-valley hydraulic gradients is possible, though the location and scale of the gradient measurement is important. Cross-valley hydraulic gradients across the hillslope-riparian transition appear to control the hyporheic extent.

4. Conclusions

[48] *Bencala et al.* [2011, p. 8] suggest "a stream is a dynamic expression of local groundwater conditions, where exchanges of water between the catchment and the channel

are continuously changing in response to heterogeneous temporal and spatial water table dynamics." Several recent studies have begun to consider coupled groundwater and stream processes. *Wondzell* [2006] reported hyporheic exchange and extent as a function of valley setting and base flow recession, using streamflow as a proxy for the hillslope-riparian-hyporheic-stream continuum. It has been proposed that hyporheic response to seasonal base flow recession is a function of both in-channel and catchment controls operating across a range of spatial and temporal scales [*Wondzell et al.*, 2010]. Further studies demonstrate the role of hillslope-riparian-stream connections as a control on the magnitude and timing of both flow rates and solute transport observed at a catchment's outlet [e.g., *Jencso et al.*, 2010]. Still, current conceptual models are only beginning to consider stream-catchment connections and their role in determining solute transport and transformation within a catchment [*Bencala et al.*, 2011]. A commonly held conceptual model in riparian hydrology suggests that increasing hydraulic gradients from the catchment toward the stream should cause hyporheic zones to contract (i.e., stronger hydraulic gradients from the stream to the hyporheic zone are necessary to overcome this ambient condition). Numerous field and numerical studies make such predictions, yet none of these studies was able to observe solute transport along flow paths in the field with high-spatial resolution.

[49] Our results suggest that the commonly held conceptual model of hydraulic gradients between the stream and groundwater, be it cross-valley hydraulic gradients toward the hillslope or vertical hydraulic gradients, as the dominant control on hyporheic exchange may be limited in its applicability, particularly in steep and narrow valleys. We found evidence of increasing hyporheic extent with both increasing and decreasing valley cross- and down-valley hydraulic gradients and with decreasing vertical hydraulic gradients. Based on our study, we conclude that characterizing hydraulic gradients at the valley bottom scale is not sufficient to predict hyporheic flow path behavior. Detailed resolution of hydraulic gradients and knowledge of their interaction with physical features of the setting are necessary to characterize hyporheic networks and their response to changing boundary conditions. It must be noted that results of this study are specific to our site; results may vary in other systems (for example, low topographic gradient streams in wide alluvial valleys might behave more consistently with conceptual models). Furthermore, we posit difficulty in assigning hydraulic gradients in steep, narrow valleys dominated with boulders and log jams as a source of uncertainty in the study.

[50] A clear contrast exists between the upper (steeper, constrained) and lower (flatter, unconstrained) sections of the study reach. Hyporheic flow paths appear rapidly in the lower valley and are persistent through late times. In the upper valley, the hyporheic network is constrained by the valley boundaries' underlying bedrock. In our study, valley constraint is a primary control on hyporheic exchange. The valley setting sets the stage upon which exchange processes at smaller scales are controlled by local hydraulic gradients, subsurface architecture (i.e., macroscale heterogeneities in the subsurface, including confining bedrock units, buried boulders and logs, etc.), and the heterogeneous distribution of hydraulic conductivity in the subsurface.

[51] We expected to find that valley-constrained hyporheic flow paths were less sensitive to changing hydrologic conditions, which was confirmed by our study. Decreased cross-valley hydraulic gradients during base flow recession had the least impact on the hyporheic area in the constrained upper reach (i.e., T1–3, where ranges of 6–11 m^2 in the peak area were observed), because control was due to subsurface structure and hydrogeologic properties rather than hydraulic gradients. Peak areas in the less-constrained lower reach (T4–5) had peak areas of approximately 14 m^2 for both transects. Despite the clear hydrologic changes through base flow recession, hyporheic extent does not follow a strong trend through the season. We conclude that hyporheic extent is not strongly related to the base flow condition in our system.

[52] We expected that decreasing cross-valley hydraulic gradients toward the stream would contribute to larger hyporheic zones. We found that steeper cross-valley hydraulic gradients were generally observed with larger hyporheic extent, in contrast to numerous studies predicting hyporheic contraction during periods with steeper cross-valley hydraulic gradients toward the stream. Finally, we expected that steeper down-valley hydraulic gradients would be related to an increased hyporheic area. We found no consistent trends with respect to down-valley hydraulic gradients.

[53] ER imaging provides an in-situ analysis of subsurface solute transport with high-spatial and temporal resolution. This data set shows the movement of tracer through hyporheic pathways in larger spatial and temporal scales than could be characterized with in-stream tracers and/or monitoring wells alone. Our ability to collect this high-resolution data in replicate studies during base flow recession allowed us to characterize both valley constraint and hydrologic gradients (e.g., base flow recession) as controls on hyporheic exchange. The ability to consider both lateral and vertical constraint due to subsurface architecture allows consideration of this type of control at a much higher-spatial resolution than past methods (i.e., transect-by-transect analysis, as compared to past studies at the valley scale). Studies in which still greater spatial resolution could be acquired would allow for increased understanding of controls on subsurface riparian hydrology. Such studies would test the spatial scale necessary for cross-, down-, and vertical-hydraulic gradients to adequately characterize the relationship between hyporheic flow paths and hydraulic gradients. The interaction of hydraulic gradients and heterogeneous hydrogeologic parameter distributions is the ultimate control on hyporheic exchange.

[54] **Acknowledgments.** Research facilities, precipitation data, and flow data were provided by the H. J. Andrews Experimental Forest research program, funded by the National Science Foundation's Long-Term Ecological Research Program (DEB 08-23380), U. S. Forest Service Pacific Northwest Research Station, and Oregon State University. This manuscript is based upon work supported by the National Science Foundation's Hydrologic Sciences program, under grant EAR-0911435. Any opinions, findings, and conclusions or recommendations expressed in this material are those of the authors and do not necessarily reflect the views of the National Science Foundation or the H. J. Andrews Experimental Forest.

References

Battin, T. (1999), Hydrologic flow paths control dissolved organic carbon fluxes and metabolism in an alpine stream hyporheic zone, *Water Resour. Res.*, *35*(10), 3159–3169.

Battin, T. (2000), Hydrodynamics is a major determinant of streambed biofilm activity: From the sediment to the reach scale, *Limnol. Oceanogr.*, *45*(6), 1308–1319.

Baxter, C., F. R. Hauer, and W. W. Wessner (2003), Measuring groundwater-stream water exchange: New techniques for installing minipiezometers and estimating hydraulic conductivity, *Trans. Am. Fish. Soc.*, *132*(3), 493–502.

Bencala, K., and R. Walters (1983), Simulation of solute transport in a mountain pool-and-riffle stream: A transient storage model, *Water Resour. Res.*, *19*(3), 718–724.

Bencala, K. E., M. N. Gooseff, and B. A. Kimball (2011), Rethinking hyporheic flow and transient storage to advance understanding of stream-catchment connections, *Water Resour. Res.*, *47*, W00H03. doi:10.1029/2010WR010066.

Binley, A., and A. Kemna (2005), DC resistivity and induced polarization methods, in *Hydrogeophysics*, edited by Y. Rubin and S. Hubbard, pp. 129–156, Springer, N. Y.

Binley, A., B. Shaw, and S. Henry-Poulter (1996), Flow pathways in porous media: Electrical resistance tomography and dye staining image verification, *Meas. Sci. Technol.*, *7*, 384.

Boano, F., R. Revelli, and L. Ridolfi (2008), Reduction of the hyporheic zone volume due to the stream-aquifer interaction, *Geophys. Res. Lett.*, *35*(9), L09401, doi:10.1029/2008GL033554.

Boano, F., A. Demaria, R. Revelli, and L. Ridolfi (2010), Biogeochemical zonation due to intrameander hyporheic flow, *Water Resour. Res.*, *46*(2), W02511, doi:10.1029/2008WR007583.

Briggs, M., M. N. Gooseff, C. D. Arp, and M. A. Baker (2008), A method for estimating surface transient storage parameters for streams with concurrent hyporheic storage, *Water Resour. Res.*, *45*, W00D27, doi:10.1029/2008WR006959.

Burt, T. (2005), A third paradox in catchment hydrology and biogeochemistry: Decoupling in the riparian zone, *Hydrol. Processes*, *19*(10), 2087–2089.

Butturini, A., and F. Sabater (1999), Importance of transient storage zones for ammonium and phosphate retention in a sandy-bottom Mediterranean stream, *Freshwater Biol.*, *41*(3), 593–603.

Cardenas, M., and J. Wilson (2007a), Dunes, turbulent eddies, and interfacial exchange with permeable sediments, *Water Resour. Res.*, *43*, W08412, doi:10.1029/2006WR005787.

Cardenas, M. B., and J. L. Wilson (2007b), Exchange across a sediment-water interface with ambient groundwater discharge, *J. Hydrol.*, *346*(3–4), 69–80.

Choi, J., J. W. Harvey, and M. H. Conklin (2000), Characterizing multiple timescales of stream and storage zone interaction that affect solute fate and transport in streams, *Water Resour. Res.*, *36*(6), 1511–1518, doi:10.1029/2000WR900051.

D'Angelo, D. J., J. R. Webster, S. V. Gregory, and J. L. Meyer (1993), Transient storage in Appalachian and Cascade mountain streams as related to hydraulic characteristics, *J. N. Am. Benthol. Soc.*, *12*(3), 223–235.

Dyrness, C. (1969), Hydrologic properties of soils on three small watersheds in the western Cascades of Oregon, *Res. Note PNW-111*, 17 pp., Pac. Northwest For. and Range Exp. Stn., For. Serv., U.S. Dep. of Agric., Portland, Oreg.

Elliott, A., and N. Brooks (1997a), Transfer of nonsorbing solutes to a streambed with bed forms: Laboratory experiments, *Water Resour. Res.*, *33*(1), 137–151.

Elliott, A., and N. Brooks (1997b), Transfer of nonsorbing solutes to a streambed with bed forms: Theory, *Water Resour. Res.*, *33*(1), 123–136.

Fabian, M. W., T. A. Endreny, A. Bottacin-Busolin, and L. K. Lautz (2010), Seasonal variation in cascade-driven hyporheic exchange, northern Honduras, *Hydrol. Processes*, *25*(10), 1630–1646, doi:10.1002/hyp.7924.

Gooseff, M., and B. McGlynn (2005), A stream tracer technique employing ionic tracers and specific conductance data applied to the Maimai catchment, New Zealand, *Hydrol. Processes*, *19*(13), 2491–2506.

Gooseff, M. N., S. M. Wondzell, R. Haggerty, and J. Anderson (2003), Comparing transient storage modeling and residence time distribution (RTD) analysis in geomorphically varied reaches in the Lookout Creek basin, Oregon, USA, *Adv. Water Resour.*, *26*(9), 925–937.

Gooseff, M. N., J. K. Anderson, S. M. Wondzell, J. LaNier, and R. Haggerty (2006), A modelling study of hyporheic exchange pattern and the sequence, size, and spacing of stream bedforms in mountain stream networks, Oregon, USA, *Hydrol. Processes*, *20*, 2443–2457, doi:10.1002/hyp.6349.

Hakenkamp, C. C., H. M. Valett, and A. J. Boulton (1993), Perspectives on the hyporheic zone: Integrating hydrology and biology. Concluding remarks, *J. N. Am. Benthol. Soc.*, *12*(1), 94–99.

Hanrahan, T. P. (2008), Effects of river discharge on hyporheic exchange flows in salmon spawning areas of a large gravel bed river, *Hydrol. Processes*, *22*(1), 127–141.

Hart, D. R., P. J. Mulholland, E. R. Marzolf, D. L. Deangelis, and S. P. Hendricks (1999), Relationships between hydraulic parameters in a small stream under varying flow and seasonal conditions, *Hydrol. Processes*, *13*(10), 1497–1510.

Hart, D., T. E. Johnson, K. L. Bushaw-Newton, R. J. Horwitz, A. T. Bednarek, D. F. Charles, D. A. Kreeger, and D. J. Velinsky (2002), Dam removal: Challenges and opportunities for ecological research and river restoration, *BioScience*, *52*(8), 669–682.

Harvey, J., and K. Bencala (1993), The effect of streambed topography on surface-subsurface water exchange in mountain catchments, *Water Resour. Res.*, *29*(1), 89–98.

Harvey, J. W., and B. J. Wagner (2000), Quantifying hydrologic interactions between streams and their subsurface hyporheic zones, in *Streams and Ground Waters*, edited by J. B. Jones and P. J. Mulholland, pp. 3–44, Academic, San Diego, Calif.

Harvey, J. W., B. J. Wagner, and K. E. Bencala (1996), Evaluating the reliability of the stream tracer approach to characterize stream-subsurface water exchange, *Water Resour. Res.*, *32*(8), 2441–2451, doi:10.1029/96WR01268.

Hynes, H. (1983), Groundwater and stream ecology, *Hydrobiologia*, *100*(1), 93–99.

Jencso, K. G., B. L. McGlynn, M. N. Gooseff, K. E. Bencala, and S. M. Wondzell (2010), Hillslope hydrologic connectivity controls riparian groundwater turnover: Implications of catchment structure for riparian buffering and stream water sources, *Water Resour. Res.*, *46*(10), W10524, doi:10.1029/2009WR008818.

Karwan, D. L., and J. E. Saiers (2009), Influences of seasonal flow regime on the fate and transport of fine particles and a dissolved solute in a New England stream, *Water Resour. Res.*, *45*(11), W11423, doi:10.1029/2009WR008077.

Kasahara, T., and S. M. Wondzell (2003), Geomorphic controls on hyporheic exchange flow in mountain streams, *Water Resour. Res.*, *39*(1), 1005, doi:10.1029/2002WR001386.

LaBrecque, D. J., and X. Yang (2001), Difference inversion of ERT data: A fast inversion method for 3-D in situ monitoring, *J. Environ. Eng. Geophys.*, *6*, 83.

Larkin, R. G., and J. M. Sharp (1992), On the relationship between river-basin geomorphology, aquifer hydraulics, and ground-water flow direction in alluvial aquifers, *Bull. Geol. Soc. Am.*, *104*(12), 1608–1620.

Meyer, J. L., W. H. McDowell, T. L. Bott, J. W. Elwood, C. Ishizaki, J. M. Melack, B. L. Peckarsky, B. J. Peterson, and P. A. Rublee (1988), Elemental dynamics in streams, *J. N. Am. Benthol. Soc.*, *7*(4), 410–432.

Morrice, J., H. M. Valett, C. N. Dahm, and M. E. Campana (1997), Alluvial characteristics, groundwater-surface water exchange and hydrological retention in headwater streams, *Hydrol. Processes*, *11*(3), 253–267.

Packman, A. I., and M. Salehin (2003), Relative roles of stream flow and sedimentary conditions in controlling hyporheic exchange, *Hydrobiologia*, *494*(1), 291–297.

Palmer, M. A. (1993), Experimentation in the hyporheic zone: Challenges and prospectus, *J. N. Am. Benthol. Soc.*, *12*(1), 84–93.

Payn, R. A., M. N. Gooseff, B. L. McGlynn, K. E. Bencala, and S. M. Wondzell (2009), Channel water balance and exchange with subsurface flow along a mountain headwater stream in Montana, United States, *Water Resour. Res.*, *45*, W11427, doi:10.1029/2008WR007644.

Peterson, E. W., and T. B. Sickbert (2006), Stream water bypass through a meander neck, laterally extending the hyporheic zone, *Hydrogeol. J.*, *14*(8), 1443–1451.

Revelli, R., F. Boano, C. Camporeale, and L. Ridolfi (2008), Intra-meander hyporheic flow in alluvial rivers, *Water Resour. Res.*, *44*(12), W12428, doi:10.1029/2008WR007081.

Runkel, R. L. (1998), One-dimensional transport with inflow and storage (OTIS): A solute transport model for streams and rivers, *U. S. Geol. Surv. Water-Resources Investigations Rep. 98-4018*, 73 pp., Denver, Colo.

Ryan, R. J., and M. C. Boufadel (2006), Influence of streambed hydraulic conductivity on solute exchange with the hyporheic zone, *Environ. Geol.*, *51*(2), 203–210.

Salehin, M., A. I. Packman, and M. Paradis (2004), Hyporheic exchange with heterogeneous streambeds: Laboratory experiments and modeling, *Water Resour. Res.*, *40*(11), W11504, doi:10.1029/2003WR002567.

Savant, S., D. D. Reible, and L. J. Thibodeaux (1987), Convective transport within stable river sediments, *Water Resour. Res.*, *23*(9), 1763–1768, doi:10.1029/WR023I009p07163.

Sawyer, A., and M. Cardenas (2009), Hyporheic flow and residence time distributions in heterogeneous cross-bedded sediment, *Water Resour. Res.*, *45*(8), W08406, doi:10.1029/2008WR007632.

Schmid, B. H., I. Innocenti, and U. Sanfilippo (2010), Characterizing solute transport with transient storage across a range of flow rates: The evidence of repeated tracer experiments in Austrian and Italian streams, *Adv. Water Resour.*, *33*(11), 1340–1346.

Slater, L., A. Binley, W. Daily, and R. Johnson (2000), Cross-hole electrical imaging of a controlled saline tracer injection, *J. Appl. Geophys.*, *44* (2–3), 85–102.

Slater, L., A. M. Binley, R. Versteeg, G. Cassiani, R. Birken, and S. Sandleberg (2002), A 3D ERT study of solute transport in a large experimental tank, *J. Appl. Geophys.*, *49*(4), 211–229.

Stanford, J. A., and J. V. Ward (1993), An ecosystem perspective of alluvial rivers: Connectivity and the hyporheic corridor, *J. N. Am. Benthol. Soc.*, *12*(1), 48–60.

Storey, R. G., K. W. F. Howard, and D. D. Williams (2003), Factors controlling riffle-scale hyporheic exchange flows and their seasonal changes in a gaining stream: A three-dimensional groundwater flow model, *Water Resour. Res.*, *39*(2), 1034, doi:10.1029/2002WR001367.

Stream Solute Workshop (1990), Concepts and methods for assessing solute dynamics in stream ecosystems, *J. N. Am. Benthol. Soc.*, *9*(2), 95–119.

Valett, H. M., J. A. Morrice, C. N. Dahm, and M. E. Campana (1996), Parent lithology, surface-groundwater exchange, and nitrate retention in headwater streams, *Limnol. Oceanogr.*, *41*(2), 333–345.

Vaux, W. G. (1968), Intragravel flow and interchange of water in a streambed, *Fish. Bull.*, *66*(3), 479.

Vervier, P., J. Gibert, P. Marmonier, and M.-J. Dole-Olivier (1992), A perspective on the permeability of the surface freshwater-groundwater ecotone, *J. N. Am. Benthol. Soc.*, *11*(1), 93–102.

Vidon, P. G. F., and A. R. Hill (2004), Landscape controls on the hydrology of stream riparian zones, *J. Hydrol.*, *292*(1–4), 210–228.

Voltz, T. J. (2011), Riparian hydraulic gradient and water table dynamics in two steep headwater streams, M.S. thesis, 167 pp., Pennsylvania State Univ., University Park, Penn.

Ward, A. S., M. N. Gooseff, and K. Singha (2010), Imaging hyporheic zone solute transport using electrical resistivity, *Hydrol. Processes*, *24*(7), 948–953.

Ward, A. S., M. N. Gooseff, and P. A. Johnson (2011), How can subsurface modifications to hydraulic conductivity be designed as stream restoration structures? Analysis of Vaux's conceptual models to enhance hyporheic exchange, *Water Resour. Res.*, *47*(8), W08512, doi:10.1029/2010WR010028.

Ward, A. S., M. N. Gooseff, and K. Singha (2012), How does subsurface characterization affect simulations of hyporheic exchange?, *Ground Water*, doi:10.1111/j.1745-6584.2012.00911.x, in press.

White, D. S. (1993), Perspectives on defining and delineating hyporheic zones, *J. N. Am. Benthol. Soc.*, *12*(1), 61–69.

Williams, D. D. (1993), Nutrient and flow vector dynamics at the hyporheic/groundwater interface and their effects on the interstitial fauna, *Hydrobiologia*, *251*(1), 185–198.

Wondzell, S. (2006), Effect of morphology and discharge on hyporheic exchange flows in two small streams in the Cascade Mountains of Oregon, USA, *Hydrol. Processes*, *20*(2), 267–287.

Wondzell, S. M., and M. N. Gooseff (2012), Exchanges/fluxes: Hyporheic, in *Treatise on Geomorphology*, vol. 9, edited by J. Schroder Jr. and E. Wohl, Academic, San Diego, Calif., in press.

Wondzell, S. M., and F. J. Swanson (1996), Seasonal and storm dynamics of the hyporheic zone of a 4th-order mountain stream. 1: Hydrologic processes, *J. N. Am. Benthol. Soc.*, *15*(1), 3–19.

Wondzell, S. M., J. LaNier, and R. Haggerty (2009), Evaluation of alternative groundwater flow models for simulating hyporheic exchange in a small mountain stream, *J. Hydrol.*, *364*(1–2), 142–151.

Wondzell, S. M., M. N. Gooseff, and B. L. McGlynn (2010), An analysis of alternative conceptual models relating hyporheic exchange flow to diel fluctuations in discharge during baseflow recession, *Hydrol. Processes*, *24*(6), 686–694.

Wright, K. K., C. V. Baxter, and J. L. Li (2005), Restricted hyporheic exchange in an alluvial river system: Implications for theory and management, *J. N. Am. Benthol. Soc.*, *24*(3), 447–460.

Wroblicky, G. J., M. E. Campana, H. M. Valett, and C. N. Dahm (1998), Seasonal variation in surface-subsurface water exchange and lateral hyporheic area of two stream-aquifer systems, *Water Resour. Res.*, *34*(3), 317–328, doi:10.1029/97WR03285.

Zarnetske, J., M. N. Gooseff, T. R. Brosten, J. H. Bradford, J. P. McNamara, and W. Breck Bowden (2007), Transient storage as a function of geomorphology, discharge, and permafrost active layer conditions in Arctic tundra streams, *Water Resour. Res.*, *43*(7), W07410, doi:10.1029/2005WR004816.

Zarnetske, J. P., R. Haggerty, S. M. Wondzell, and M. A. Baker (2011), Dynamics of nitrate production and removal as a function of residence time in the hyporheic zone, *J. Geophys. Res.*, *116*(G1), G01025, doi:10.1029/2010JG001356.

A. M. Binley, Lancaster Environment Centre, Lancaster University, Lancaster LA1 4YQ, UK.

M. Fitzgerald and K. Singha, Department of Geosciences, Pennsylvania State University, 505 Deike Bldg., University Park, PA 16802, USA.

M. N. Gooseff and T. J. Voltz, Department of Civil and Environmental Engineering, Pennsylvania State University, 202 Sackett Bldg., University Park, PA 16802, USA.

A. S. Ward, Department of Geoscience, University of Iowa, 121 Trowbridge Hall, Iowa City, IA 52242, USA. (adam-ward@uiowa.edu)

Correction to "Hydrologic and geomorphic controls on hyporheic exchange during baseflow recession in a headwater mountain stream"

Adam S. Ward, Michael Fitzgerald, Michael N. Gooseff, Thomas J. Voltz, Andrew M. Binley, and Kamini Singha

Received 11 July 2012; published 17 August 2012.

Citation: Ward, A. S., M. Fitzgerald, M. N. Gooseff, T. J. Voltz, A. M. Binley, and K. Singha (2012), Correction to "Hydrologic and geomorphic controls on hyporheic exchange during baseflow recession in a headwater mountain stream", *Water Resour. Res.*, *48*, W08903, doi:10.1029/2012WR012663.

1. Introduction

[1] In the paper "Hydrologic and geomorphic controls on hyporheic exchange during baseflow recession in a headwater mountain stream" by Adam S. Ward et al. (*Water Resources Research*, *48*, W04513, doi:10.1029/2011WR011461, 2012), the inverse modeling of electrical geophysical data is described in section 2.4.2 as follows: "Data collected during and after the tracer injection were inverted using the background model as a starting model. Thus, each time step was inverted independently [as by *Ward et al.*, 2010, 2012]. Time lapse-inversion [e.g., *LaBrecque and Yang*, 2001], or inversion of differences might provide some improvement in the results and should be considered for future studies." This description is incorrect. The results presented do use the background (pretracer) model as a starting model, as stated, but the inversion used was the difference inversion of *LaBrecque and Yang* [2001]. Briefly, this is a modified version of the Occam's inverse method where the inversion seeks the change in subsurface model parameters from the starting model by inverting on the change in observed electrical data, conditioned on a reference model parameter set (in this case, the pretracer model). These inversion techniques were selected to reduce artifacts in the time lapse images and to minimize systematic errors in the inversion models (e.g., errors arising from electrode configuration and model discretization).

References

LaBrecque, D. L., and X. Yang (2001), Difference inversion of ERT data: A fast inversion method for 3-D in situ monitoring, *J. Environ. Eng. Geophys.*, *6*(2), 83–89, doi:10.4133/JEEG6.2.83.

Ward, A. S., M. N. Gooseff, and K. Singha (2010), Imaging hyporheic zone solute transport using electrical resistivity, *Hydrol. Processes*, *24*(7), 948–953, doi:10.1002/hyp.7672.

Ward, A. S., M. N. Gooseff, and K. Singha (2012), How does subsurface characterization affect simulations of hyporheic exchange?, *Ground Water*, doi:10.1111/j.1745-6584.2012.00911.x, in press.

0043-1397/12/2012WR012663